Atmos. Chem. Phys. Discuss., https://doi.org/10.5194/acp-2018-944
Manuscript under review for journal Atmos. Chem. Phys.
Discussion started: 17 October 2018

Atmospheric Chemistry and Physics Discussions

Weak and intense katabatic winds: impacts on turbulent characteristics in the stable boundary layer and CO_2 transport

Jon A. Arrillaga[1], Carlos Yagüe[1], Carlos Román-Cascón[1,2], Mariano Sastre[1], Gregorio Maqueda[1], and Jordi Vilà-Guerau de Arellano[3]

[1]Dept. Física de la Tierra y Astrofísica, Universidad Complutense de Madrid, Spain
[2]Laboratoire d'Aérologie, University of Toulouse, CNRS, France
[3]Meteorology and Air Quality Group, Wageningen University, Netherlands

Correspondence: Jon A. Arrillaga (jonanarr@ucm.es)

Abstract. The role of thermally-driven local downslope or katabatic flows in the dynamics and turbulent features of the stable boundary layer (SBL) is investigated using observations. Measurements are carried out in a relatively flat area 2-km away from the steep slopes of the Guadarrama Mountain Range (Spain). Forty katabatic events are selected from an observational database spanning the 2017-summer period, by using an objective and systematic algorithm that is able to account for local and synoptic forcings. We subsequently classify the katabatic events into weak, moderate and intense according to the observed maximum wind speed. This classification enables us to contrast the main differences in dynamics and thermal structure. We find that the stronger katabatic events are associated with an earlier onset time of these flows. We relate it to very low soil-moisture values (< 0.07 m^3 m^{-3}, i.e. smaller than the median during the analysed period) and a weak synoptic wind ($V_{850} < 6$ m s^{-1}) having the same direction as the katabatic. The relative flatness of the area favours the formation of very stable boundary layers characterized by a longwave radiative cooling of around 60-70 W m^{-2} and very weak turbulence (friction velocity (u_*) < 0.1 m s^{-1}). They occur when katabatics are weak, and are occasionally associated with the formation of skin flows, that are manifested as weak jets ($U < 1$ m s^{-1}) at 3 m. Intense katabatics, instead, are characterised by a strong and increasing bulk shear (the maximum u_* is close to 1 m s^{-1}) that avoids the development of the surface-based thermal inversion, giving rise to the so-called weakly stable boundary layer. We identify the transition between the two regimes for a threshold katabatic wind speed of around 1.5 m s^{-1}, in agreement with the hockey-stick transition hypothesis. Our analysis is extended by calculating non-dimensional numbers to characterize the transition: the shear capacity, the bulk Richardson number and z/L. On the other hand, by inspecting individual weak and intense events, we further explore the interaction between katabatic flows and turbulence, and the impact on CO_2 concentration. By relating the dynamics of the two regimes with the CO_2 budget, we are able to estimate the contribution of the different terms. For the intense event, indeed, we infer a horizontal transport of 67 ppm in 3 h driven by the katabatic advection.

1 Introduction

Thermally-driven slope winds develop in mountainous areas, when the large-scale flow is weak and skies are clear, allowing greater incoming solar radiation during daytime and larger outgoing longwave radiation during the night (Zardi and Whiteman, 2013). Under this situation, wind direction is reversed twice per day: thermally-driven winds flow upslope during the day

and downslope during the night (Atkinson, 1981; Whiteman, 2000; Poulos and Zhong, 2008). The thermal disturbances that produce them have different scales and origin: from local hills and shallow slopes (Mahrt and Larsen, 1990) to large basins and valleys which extend horizontally up to hundreds of kilometers (Barry, 2008). The different scales, however, are not independent; for instance, local downslope flows converge at the bottom of the valleys generating larger-scale flows, which in turn influence the mountain-plain circulations.

Mountainous sites have striked the attention of many studies for plenty of reasons: in particular due the influence on the formation of fogs (Hang et al., 2016), diffusion of pollutants (Li et al., 2018), and also due to the important role that slope flows play in the thermal and dynamical structure of the Atmospheric Boundary Layer (ABL) and its morning and evening transitions (Whiteman, 1982; Sun et al., 2006; Lothon et al., 2014; Lehner et al., 2015; Román-Cascón et al., 2015; Jensen et al., 2017).

In this work, we focus on the thermally-driven local downslope winds (hereinafter *katabatic flows*) and on their role during the afternoon and evening transition of the ABL, affecting the turbulent characteristics of the Stable Boundary Layer (SBL) and the transport of CO_2. Despite the term *katabatic* is also used for refering to other non-thermally-driven winds (Zardi and Whiteman, 2013), by following Barry (2008) we use it to refer to downslope winds driven by local thermal disturbances (i.e. not by the basin or valley). Several external factors have been documented to affect katabatic winds: the steepness of the slope and the distance to the mountain range (Horst and Doran, 1986), the canopy layer (Sun et al., 2007), spatial variations in soil moisture (Banta and Gannon, 1995; Jensen et al., 2017), and the direction and intensity of the synoptic wind (Fitzjarrald, 1984; Doran, 1991). However, most of the investigations analysing the influence of those external factors are carried out using numerical simulations, and there is a lack of observational studies to validate them. Hence, we firstly try to corroborate the findings from numerical experiments, particularly on how soil moisture and the large-scale wind affect the onset time and intensity of katabatic winds, from an observational analysis of several katabatic events. By way of example, Banta and Gannon (1995) carried out numerical simulations using a two-dimensional model and found that katabatic flows are weaker over a moist slope than over a dry one. They quantified a greater downward longwave radiation and soil conductivity under moister conditions, which gives rise to a reduced surface cooling. However, Jensen et al. (2017) found an opposite correlation, which they atributted to the sensitivity of the soil-moisture parametrisation in the numerical simulations. As a matter of fact, Sastre et al. (2015) showed with a numerical experiment in contrasting sites that soil moisture differences do not affect the afternoon and evening transition values with the same intensity, but depending on the site. With respect to the background flow, by using a one-dimensional model Fitzjarrald (1984) observed that the onset time of katabatic winds is affected by the retarding effect of the opposing synoptic flow and reduced cooling rates. Our observational analysis aims at shedding light on the influence of those two external factors.

On the other hand, knowing whether a certain night katabatics will be weak or intense enables us to predict how turbulence in the SBL will behave. It is well known that under weak large-scale wind, turbulence is weak and patchy (Van de Wiel et al., 2003, 2012a; Mahrt, 2014), giving rise to the so-called very stable boundary layer. On the contrary, when the large-scale wind is strong, shear production increases substantially and turbulence is continuous, producing near-neutral conditions in the SBL (Mahrt, 1998; Sun et al., 2012; Van de Wiel et al., 2012b), and the so-called weakly stable boundary layer. Being able to foresee

the occurrence of these two regimes has been in the eye of many studies, and some attempts have been made to characterise the transition between the regimes using diverse criteria such as the geostrophic wind (van der Linden et al., 2017), local (Mahrt, 1998) and non-local scaling parameters (van Hooijdonk et al., 2015), and the wind speed (Sun et al., 2012). More or less directly continuous turbulence in the SBL has been linked with a stronger background wind (e.g. > 5–7 m s^{-1} in Van de Wiel et al. (2012b)) and low-level jets (Sun et al., 2012), or even with occasional irruption of sea-breeze fronts (Arrillaga et al., 2018).

Our aim is to explore the direct implication of katabatic winds generated by the presence of steep topography, in the occurrence of the two SBL regimes. A relevant aspect of our emplacement is its location in a relatively small flat area nearby the mountain range. We therefore encounter a scenario different from other sites located at slopes where the SBL barely becomes very stable, since the shear production linked with the katabatic is large and continuous, and buoyant turbulence production may occur even when the stable stratification is present (Oldroyd et al., 2016). In our emplacement, however, very stable boundary layers associated with relatively strong surface-based thermal inversions take place occassionally. Besides, over flat or almost flat terrain universal scaling according to Monin-Obukhov Similarity Theory (MOST) can be applicable and corrections due to measuring over a slope are not required (Stiperski and Rotach, 2016).

Connected also to the dynamics of the SBL, another relevant issue on this topic is the impact of katabatic winds in the concentration of scalars of high relevance such as the CO_2. Previous studies have documented its influence at coastal areas (Cristofanelli et al., 2011; Legrand et al., 2016) and mountainous regions (Sun et al., 2007). Advection driven by katabatic winds can indeed dominate the total CO_2 transport; for instance, Sun et al. (2007) found that downslope flows transported CO_2-rich air from the Rocky mountains. Not only advection, but local turbulence fluxes can also be influenced: Sun et al. (2006) observed an anomalous positive CO_2 flux just after sunset, suggesting that it was due to the sudden transition from upslope to downslope flow. Being able to better quantify the influence of mesoscale flows on the CO_2 budget can help to reduce the large discrepancy from modelling studies in reproducing the land-atmosphere exchange for this gas (Rotach et al., 2014).

For the above-mentioned reasons, the main aspects that motivate research in this study, in short, are the following:

[1] The external factors that modulate the onset of katabatic flows and yield to different intensities.

[2] The interaction of katabatic winds with local turbulence in the SBL and the implication in turbulent characteristics.

[3] The role of katabatic advection and local turbulent fluxes, associated with the distinct SBL regimes, in CO_2 mixing ratio.

In order to shed light on those aspects, we perform an objective selection of katabatic events and group them together according to their maximum wind speed, so that their intensity and the turbulent characteristics of the SBL are clearly associated. The article is structured as follows. We detail the observational data employed and the objective criteria for selecting katabatic events in Section 2. Section 3 addresses the principal characteristics of these events and explores the influencing factors. We pursue the interaction with turbulence and the link with the different regimes in the SBL in Section 4. Section 5 deepens the analysis by inspecting in detail two individual events, and estimates the contribution of the horizontal transport to the variability of the CO_2. We finish with the relevant conclusions.

Atmos. Chem. Phys. Discuss., https://doi.org/10.5194/acp-2018-944
Manuscript under review for journal Atmos. Chem. Phys.
Discussion started: 17 October 2018

2 Data & Method

2.1 Site: La Herrería

The emplacement for the observations used in this work (meteorological, soil and CO_2 mixing ratio) is located beside *La Herrería* Forest (40.582° N, 4.137° W, 920 m asl), from which the name is adopted. La Herrería is placed at the foothills of the Guadarrama Mountain Range in central Spain, approximately 50 km NW of the city of Madrid (see Fig. 1a). The emplacement chosen is a key aspect for the study carried out for various reasons explained below.

First, it is placed at around 2 km from the steep slope of the Guadarrama mountain range (see Fig. 1b), which has an slope angle of around 25° in the main katabatic direction (295°; approximately W-NW, from which the most intense katabatic winds blow). The closest peak, Abantos, is 1763 m high, and the summit Peñalara is at 2420 m asl; both pointed in Fig. 1a. Second, it is close to a highly vegetated area to the W, being also close enough to the small urban areas of San Lorenzo de El Escorial to the NW and El Escorial to the E-SE. In addition, it is relatively close to the large metropolitan area of Madrid, where concern regarding high pollution levels has increased in the last years (Borge et al., 2016, 2018). The diffusivity of pollutants is highly affected by the presence of down-basin winds in the city (Plaza et al., 1997), which develop from converging katabatic flows at the centre of the basin. Besides, the generation of katabatic drainages causes fog formation in the centre of the Iberian Peninsula, affecting visibility, amongst others, in Madrid-Barajas Adolfo Suárez airport (Terradellas and Cano, 2007). Understanding the factors that modulate katabatic winds in this region is therefore of high importance. Third, the analysis is carried out during summer, a season that is characteristically very dry and warm in central Spain, even at the mountainous areas (Durán et al., 2013). The soil is particularly dessicated at the end of the season, which makes it different from other mountainous areas in Europe as the Pyrenees or the Alps. Summer 2017 was very warm and very humid (AEMET, 2017) in this region, following a very warm and very dry spring. In any case, it was not a particularly rainy season and in fact, precipitation during summer 2017 took place just over a few days, so that the dessicated soil experienced sharp moisture increases. This sets up a striking working frame to explore the role of soil moisture in the surface-energy balance and the impact on the intensity of katabatic flows. And finally, the area surrounding the station is located in an relatively flat area (its slope angle is of around 2°) immediately besides the mountain range (see Fig. 1b), which allows the formation of strong surface thermal inversions. These inversions are sporadically eroded by the arriving katabatic flows, providing an interesting scenario for the investigation of the distinct SBL regimes.

Regarding the vegetation and land use, the observational site is placed in a pasture grassland with scattered 3–4 m high shrubs, and the soil is composed of granite and gneiss. At around 2 km towards the SW, a broadleaved decidious forest is found, and at the same distance to the NW, approximately where the steep slope starts, a mixture of needleleaved evergreen tree cover and mosaic-tree and herbaceous cover. During the katabatic stage, the footprint can reach horizontally up to 200 m, lying within the fetch of the station (Arrillaga et al., 2016). Nevertheless, under very stable conditions the footprint may increase substantially, which could induce uncertainty in the estimation of the turbulent fluxes and a possible impact of the urban area located to its NW. In any case, the direct implications of the urban area are negligible given the little traffic and the inexistent industrial activity.

Atmos. Chem. Phys. Discuss., https://doi.org/10.5194/acp-2018-944
Manuscript under review for journal Atmos. Chem. Phys.
Discussion started: 17 October 2018

Atmospheric Chemistry and Physics Discussions

2.2 Data: Meteorological observations

Eddy-covariance fluxes of energy, moisture and CO_2, and standard meteorological measurements are recorded over the warmest and driest season of the year, when thermally-driven slope winds are strongest and weak large-scale winds prevail.

La Herrería tower is part of the Guadarrama Monitoring Network (GuMNet, GuMNet (2018)), which aims at providing observational meteorological and climatological records to deepen into scientific research in the mountainous area of *Sierra de Guadarrama* (Durán et al., 2018). We record data from aspirated thermometers, cup anemometers, a wind vane and IRGASON devices among others in a 10-m high fixed tower. From the IRGASON equipment the three components of the wind, temperature and CO^2 measurements are obtained at high frequency (10 Hz), which allows the evaluation of different turbulent fluxes. Measurements of the radiation components and the soil heat flux(G), as well as the calculated sensible-heat (H) and latent-heat (LH) fluxes, allow the analysis of the surface energy balance as well.

Measurements were carried out over an intensive campaign in Summer 2017 (22/06–26/09), with supplementary vertical levels. Table 1 gathers specifications about the devices and the variables employed in this study. Depending on the instrumentation used and the variables measured, different sampling rates were employed. This information is also provided in Table 1. On the other hand, all the variables employed in this analysis are averaged over 10 min.

2.3 Method: Katabatic-detection criteria

The research strategy from Arrillaga et al. (2018), in which they applied an objective and systematic algorithm to the observational data in order to select sea-breeze events, is followed. In this work, we adjust the algorithm for selecting events that fulfil predefined katabatic criteria. In this way, we evaluate the characteristics and impacts of the katabatic flows in a more robust and objective way. Besides, the algorithm defines a benchmark which is the onset of the katabatic flow, enabling the clustering of different events and their analysis in a consistent way.

The algorithm consists of four different filters, which are shown in Table 2. The first three are coincident with the algorithm defined in Arrillaga et al. (2018), just modifying the precipitation-amount threshold for Filter 3: 0.5 instead of 0.1 mm/day, since weak and scattered showers (< 0.5 mm) do not alter the onset and development of katabatic winds. From detailed individual analysis we found that the large-scale conditions favourable for the formation of katabatic flows are those that apply for sea breezes, i.e. quiescent synoptic forcing and not having the passage of synoptic fronts (Filters 1 and 2 respectively). This fact supports the strong value of this method. The last filter (Filter 4) is based on specific criteria for katabatic flows in La Herrería, and was defined after a thorough inspection of the wind behaviour around sunset on days passing the first three filters. An event is selected as 'katabatic' when wind direction at 10 m is roughly perpendicular to the mountain-range axis, i.e. within the range [250°–340°], for at least 2 hours at a time between 1600 UTC and 2400 UTC (1800 and 0200 LT respectively). The katabatic flow usually lasts until sunrise, when a strong veering of the wind direction occurs. However, in this study we just focus on the first stage of these flows, since the main objective is to investigate their connection with the onset of the SBL (defined as when the sensible heat flux, H, turns negative), and the different regimes associated. During the summer months, the katabatic onset usually takes place before sunset around 1800 UTC, but it can be considerably advanced or delayed depending on a number of

Atmos. Chem. Phys. Discuss., https://doi.org/10.5194/acp-2018-944
Manuscript under review for journal Atmos. Chem. Phys.
Discussion started: 17 October 2018

Atmospheric Chemistry and Physics Discussions

factors, which are investigated in Sec. 3.2. A wide variability in the onset time of the katabatic flow was also reported in the studies from Pardyjak et al. (2009) and Nadeau et al. (2013).

We identify the onset of the katabatic flow as the first value within the 2-h range of continuous katabatic direction. Having that onset time as a reference, we explore the characteristics of katabatic flows, their interaction with turbulence and the impact on CO_2 in the next sections.

3 Characteristics of the katabatic flows

Forty were selected as days with the formation of katabatic events from the analysed summer period with available data (94 days in total). The algorithm is very rigorous to ensure that the selected events are strictly thermally driven downslope flows and not dynamically driven, since we just focus on the days with a weak large-scale wind in which there is a shift from the daytime upslope to the night-time downslope wind direction. The results presented hereinafter are related to these 40 katabatic events.

3.1 Wind direction and intensity

Fig. 2 shows the direction and intensity of the katabatic events over the 2-h period subsequent to the onset of the downslope flow. The mean katabatic direction is around 290–300° and the variation around this direction is small; the largest oscillations in the direction are observed for weak intensities. Within the database of the 40 events we find diverse cases depending on the maximum intensity of the katabatic flow. We represent in Fig. 3 the wind vertical profile at the time of the katabatic onset (a) and when the katabatic intensity is maximum (b) using box plots, which contain information about the frequency distribution at each observational level (3, 6 and 10 m). At the time of the onset the katabatic flow is weak at all levels (Fig. 3a); for instance the median at 10 m is slightly over 1 m s^{-1}. It can be noted that the median at 3 m is similar to that at 6 m, and the first quartile is even smaller at 6 m. This occurs because prior to the identified onset at 10 m a very shallow katabatic or a skin flow is usually developed, and is only reflected at 3 m (as observed for instance in Román-Cascón et al. (2015)). This skin flow can be observed when turbulence is very weak and thermal stratification is very stable (Mahrt et al. 2001; Soler et al. 2002), and occasionally gives rise to a greater wind speed at 3 than at 6 m, few times even greater than at 10 m. However, when the katabatic flow is more intense, wind speed increases with height within the 10-m layer from the surface (for instance note that the third quartile is greater at 6 than at 3 m). A maximum jet is probably found above 10 m.

When the maximum katabatic intensity at 6 m is represented (Fig. 3b) the distribution above the median is elongated at all levels. In fact, the level of 6 m is employed to classify katabatic events according to the their maximum intensity and the associated erosion of the surface-based thermal inversion. The reasons for employing the level of 6 m are outlined below. Firstly, red crosses pinpoint an event identified as an outlier due to its high intensity at all levels (e.g. $U > 6$ m s^{-1} at 10 m). Together with the wind maximum, the surface thermal inversion is very weak or inexistent, and the maximum of turbulence measured from the turbulent kinetic energy ($TKE = [(1/2)(\overline{u'^2} + \overline{v'^2} + \overline{w'^2})]^{(1/2)}$) and friction velocity ($u_* = [(\overline{u'w'})^2 + (\overline{v'w'})^2]^{1/4}$) is even greater than the daytime maximum of the typical diurnal cycle (generally $u_* \simeq 0.5$–0.7 m s^{-1}). We find in addition two

Atmos. Chem. Phys. Discuss., https://doi.org/10.5194/acp-2018-944
Manuscript under review for journal Atmos. Chem. Phys.
Discussion started: 17 October 2018

Atmospheric Chemistry and Physics Discussions

other events with the above-mentioned features which are included within the right whisker. These three events are classified hereinafter as intense katabatics, and they all meet that the maximum 10-minutal wind speed at 6 m is greater than 3.5 m s^{-1}. Secondly, in some events turbulence is very low and the surface-based thermal inversion is not eroded ($u_* < 0.1$ m s^{-1}). They all occur when wind speed is very weak, and hence we classify as weak events (14 in total) those in which the maximum wind speed at 6 m is below 1.5 m s^{-1}. The cases in which the maximum wind speed at 6 m is between 1.5 and 3.5 m s^{-1} are classified as moderate katabatics (23 in total). A summary of the classification is shown in Table 3. We employ the level of 6 m for the classification, since at 3 and 10 m the events showing different features cannot be so clearly detached. Flocas et al. (1998) for instance studied katabatic flows at a similar height (7 m), since the influence of the large-scale wind was minimised at this level.

This classification is employed in the following sections to better illustrate the differences between the katabatic events, and the very distinct way in which they interact with local turbulence (in particular this is addressed in Secs. 4 and 5).

3.2 Factors influencing intensity

Once the katabatic events are classified according to their maximum intensity, we explore the factors that induce different intensities. Fig. 4 shows a histogram with the difference between the onset time of the katabatic flow and sunset time (it ranges from 1810 UTC in September to 1940 UTC in June), for different intensities in colours, and in lines for different thermal stratification at the moment of the onset. To calculate the thermal stratification we fitted the virtual potential temperature at the different vertical levels (soil, 3, 6 and 10 m) to a logarithmic profile. The soil temperature was calculated from the upward longwave radiation. The fitting was carried out as follows:

$$\theta_v(z,t) = \alpha(t) + \beta(t)ln(z) + \gamma(t)ln^2(z) + \delta(t)ln^3(z). \tag{1}$$

The type of thermal stratification is inferred from the value of δ at the moment of the onset, and subsequently classified into the subsequent three groups:

$$\begin{aligned} Unstable: &\quad \delta(t = onset) < -0.3\ Km^{-3}, \\ Neutral: &\quad -0.3\ Km^{-3} \leq \delta(t = onset) \leq 0\ Km^{-3}, \\ Stable: &\quad \delta(t = onset) > 0\ Km^{-3}. \end{aligned} \tag{2}$$

From this classification we infer the relationship between the earlier or later onset of the katabatic wind, thermal stratification at the moment of its onset and the intensity of the flow. On the one hand, intense katabatics develop when the onset takes place prior to 2 hours before sunset and the stratification in the first 10 m is still unstable. On the other, weak katabatics occur when the onset takes place later than 2 hours before sunset and with neutral or stable stratification. Moderate katabatics, however, can occur either earlier or later independently of the stratification.

Linked with the three different thermal-stratification regimes defined in Eq. 2, we explore the influence of the TKE at the onset of katabatic flows from Fig. 5a. By representing the maximum katabatic intensity at 6 m with respect to the TKE at the

Atmos. Chem. Phys. Discuss., https://doi.org/10.5194/acp-2018-944
Manuscript under review for journal Atmos. Chem. Phys.
Discussion started: 17 October 2018

Atmospheric Chemistry and Physics Discussions

onset, two main groups result. In one of them TKE is very low at the onset (in the order or smaller than 0.1 m^2 s^{-2}), which includes all the weak katabatics. This group is associated with a later onset of the katabatic flow (Fig. 4), when the thermal stratification is already neutral or stable and R_{net} < 40 W m^{-2} always; it is in fact negative in more than 80 % of the cases. On the other group, TKE is about one order of magnitude greater and includes all the intense events, which are related with an earlier katabatic onset, when the thermal stratification is already unstable. R_{net} is in fact always > 80 W m^{-2} at the onset.

This result implies that there is a strong relation between katabatic flows and turbulence, which is essential to fully understand their nature and development. This aspect is further addressed in Sect. 4. Regarding the moderate katabatics, we separate them into two subgroups: $U_{max} \leq 2.5$ m s^{-1} (triangles pointing downward) and $U_{max} > 2.5$ m s^{-1} (triangles pointing upward). Even though the weaker moderate katabatics are mostly related with the stable and neutral stratification and the more intense moderate with the unstable stratification, the opposite occurs also in few of the cases. This result suggests the existence of external factors affecting the earlier or later onset of katabatic winds. For the reasons outlined in the introduction, we investigate two factors: soil moisture and the large-scale wind.

To explore the influence of soil moisture, we define an index that provides a measure of the relative dessication of the soil over the summer. This soil-moisture index is defined as the ratio between the observed liquid water volume and the maximum value throughout the analysed period (0.14 m^3 m^{-3}): $SM_i = SM/SM_{max}$. We separate the events into drier ($SM_i \leq 0.5$) and moister ($SM_i > 0.5$) cases. On the other hand, to explore the influence of the large-scale wind ($V_{850,18}$: at 850 hPa at 18 UTC) despite its low intensity required by the selection algorithm, we separate the katabatic events into very weak ($V_{850,18} \leq 3.5$ m s^{-1}) and weak ($V_{850,18} > 3.5$ m s^{-1}) synoptic forcing.

The influence of the large-scale wind speed and direction, and soil moisture are investigated in Fig. 6. The maximum katabatic intensity at 6 m together with the direction of the synoptic wind are represented in wind-rose form for the abovementioned drier (a,b) and moister (c,d) cases, and for a very weak (a,c) and weak (b,d) synoptic forcing. The synoptic wind is estimated from the NCEP reanalysis wind speed employed in the selection algorithm, by choosing the grid point at 850 hPa closest to La Herrería (40.5° N, 4° W) at 18 UTC. At that point, the 850-hPa level is approximately at 800 m agl, sufficiently close to the surface as to be representative of the synoptic wind at the surface level, and far enough as to be out of the influence of katabatic flows. We find that intense katabatics (orange-reddish) develop when the soil is drier, the large-scale wind is weak and blowing from the N-NW (Fig. 2b). This direction is perpendicular to the mountain range axis (Fig. 1a), and approximately coincident with the katabatic direction (Fig. 2). However, under those conditions we find weak katabatics (dark blue) when the large-scale wind blows from parallel or opposite directions (S or E-NE for instance), although most of the weak katabatics occur mainly when the soil is moister and the synoptic forcing is very weak (Fig. 2c). Weak katabatics establish primarily for W-SW and S-SE large-scale winds, but they can also occur for N-NW winds when their intensity is very weak (Fig. 2a). Overall, the intensity of katabatics increases with decreasing soil moisture, and increasing synoptic forcing with a N-NW direction.

To study the role of the soil moisture and the relative dessication of the soil in the surface energy balance, we represent the observed average G and longwave-radiative loss ($LWU–LWD$) during the katabatic stage with respect to the SM_i in Figure 7. To better show the trends of the scatter plots, a 4-th order polynomial fitting has been added. Both G and $LWU–LWD$ show two maxima for high and low SM_i, at around 0.9 and 0.2–0.3 respectively. The peak for low SM_i is more pronounced, and implies

Atmos. Chem. Phys. Discuss., https://doi.org/10.5194/acp-2018-944
Manuscript under review for journal Atmos. Chem. Phys.
Discussion started: 17 October 2018

Atmospheric Chemistry and Physics Discussions

that the cooling of the soil is stronger when the relative dessication is higher, since the average G is positive (opposing to $G < 0$ for the secondary peak) and the longwave-radiative loss is greater. However, when the soil moisture increases considerably after precipitation has occurred ($SM_i \simeq 0.9$), the cooling of the soil can also be enhanced, inducing an enlarged thermal contrast between the slope and the overlying air layer, and therefore contributing to the intensification of the katabatic flow. The contrasting findings from Banta and Gannon (1995) and Jensen et al. (2017) for the impact of the soil moisture in the katabatic intensity could be explained by this bimodal behaviour.

Overall, we can conclude that the combination of low soil moisture and synoptic wind direction coincident with the downslope direction (N-NW) induces an earlier onset of katabatic flows, when stratification is still unstable and convective turbulence relatively strong, which facilitates the development of intense katabatic flows. If those conditions are not met, the onset occurs later when stratification is already neutral or stable, which limits the intensification of katabatic flows. Nevertheless, sharp enhancements in the soil moisture due to precipitation can give rise to a stronger cooling of the soil and an earlier onset of the katabatic flow. To understand the evolution of katabatic flows after their onset we explore their interaction with turbulence in the next section.

4 Interaction between katabatics and turbulence

Thermal stratification and the associated turbulence at the moment of the onset modulate the intensity of the katabatic flow. If the katabatic flow arrives when the stratification is still unstable and the surface thermal inversion (hereinafter measured from $\Delta\theta_v$) is not formed yet, the shear associated with the katabatic flow increases, and the downslope flow strengthens progressively. Later, due to radiative energy loss ($R_{net} < 0$) the stable stratification is already established ($\Delta\theta_v > 0$). Given that turbulence associated with wind shear is already high, the negative H strengthens ($H < 0$) and after a while compensates the energy loss at surface, impeding the development of the surface-based inversion and inducing near-neutral stability conditions. In that way, intense katabatics give rise to a weakly stable boundary layer. On the other hand, if the katabatic wind arrives later and thermal stratification is already neutral or stable, the increase of shear is limited by the stable stratification itself. Thus, even the maximum sustainable heat flux does not compensate the radiative energy loss. Consequently, the bottom of the SBL cools down, which contributes to enhance the stable stratification. This positive feedback occurring under weak katabatics suppresses turbulence and gives rise to a very stable boundary layer. For moderate katabatics, any of the two regimes can occur depending on the onset time and the surface-energy balance. These mechanisms are explored below by means of measured variables and calculated nondimensional relevant parameters.

4.1 Turbulence regimes in the SBL

Figure 8 shows the temperature stratification $\Delta\theta_v$ and the turbulence velocity scale V_{TKE} *vs* U at 6 m. In this and subsequent figures we just represent the 10-min average values (just until 24 UTC) in which the wind direction is katabatic and H is negative, so that the katabatic flow is present and the SBL is already established. V_{TKE} is calculated as the root square of the TKE. By representing $\Delta\theta_v$ *vs* U we find a contrasting relationship for weak and intense katabatics (Fig. 8a). Weak katabatics

Atmos. Chem. Phys. Discuss., https://doi.org/10.5194/acp-2018-944
Manuscript under review for journal Atmos. Chem. Phys.
Discussion started: 17 October 2018

Atmospheric Chemistry and Physics Discussions

give rise to a strongly stratified SBL ($\Delta\theta_v$ up to 2 K), whereas intense katabatics are linked with very weak or almost inexistent surface-based thermal inversions. Interestingly, for few 10-minutal values with similar wind speed ($U \simeq$ 1–1.5 m s^{-1}) the thermal stratification is very different between weak and intense katabatics, which suggests the existence of distinct regimes in the SBL. On the other hand, we find for very weak wind speed ($U <$ 1 m s^{-1}) a large variability of thermal stratification, that occurs because around the onset of katabatics the thermal inversion is still absent or very weak in most of the cases. At the upper limit, however, $\Delta\theta_v$ tends to zero when wind speed increases its value. Moderate katabatics show both types of behaviour, with the transition taking place for $U \simeq$ 1.5 m s^{-1}.

By representing the turbulence strength V_{TKE} *vs* U at 6 m we confirm the sharp transition for U = 1.5 m s^{-1} (Fig. 8b). Weak katabatics are associated with very weak turbulence ($V_{TKE} <$ 0.5 m s^{-1}) that hardly increases with wind speed, while turbulence for intense katabatics is considerably greater and increases linearly with U. This behaviour was first observed in Sun et al. (2012), and defined as the HOckey-Stick Transition (HOST) in Sun et al. (2015). They identified three turbulence regimes in the SBL depending on the relationship between turbulence and wind speed. In regime 1 turbulence is very weak and generated by local shear; in regime 2 turbulence is strong and generated by the bulk shear U/z (hence the linear relationship with wind speed); and finally, in regime 3 turbulence is moderate and mainly generated by top-down turbulent events. The three regimes are pinpointed in Fig. 8b. The threshold value for the wind speed depends on height, and sets the value above which the abrupt transition from regime 1 to regime 2 occurs. Since in our case z = 6 m, it is indicated as V_6 in the figure. Weak katabatics are clearly associated with regime 1 and intense katabatics, instead, with regime 2. Moderate katabatics can give rise to either the three of the regimes. We just show the relationship for z = 6 m, and HOST in our case occurs for V_6 = 1.5 m s^{-1}, which is significantly lower than the value at that height from Sun et al. (2012) ($\simeq$ 3 m s^{-1}) over relatively flat and homogeneous terrain (Poulos et al., 2002). Besides, V_6 coincides with the threshold value we anticipated for defining weak katabatics (Table 3). We measure a slope of ∼0.5 for *VTKE* vs U for regime 2, while is of ∼0.25 in the results from Sun et al. (2012).

In Fig. 9 we explore how katabatic intensities and turbulence strength are manifested in terms of heat flux. The downward H (i.e. when the SBL is already established: $H < 0$) is represented with respect to U at 6 m in Fig. 9. The smallest H values are observed for weak katabatics, when $U <$ 1 m s^{-1}. The highest values take place for moderate katabatics when U lies between 1.5–2.5 m s^{-1}. We find a few data from some intense katabatics in which H is nearly 0 for that wind-speed range, when the thermal inversion is still very weak. For intense katabatics the peak is reached at $U \simeq$ 3 m s^{-1}, and above that intensity H decreases, since it is limited by the neutral stratification. One of the key questions is whether this heat flux is able to compensate the surface radiative loss. This matter is addressed later in Sect. 5.1 by analysing the time evolution of the surface-energy balance on individual events.

4.2 Regime transition from non-dimensional parameters

We have observed in Sect. 4.1 that the nocturnal regime can be predicted from the katabatic intensity at 6 m. In fact, by knowing in advance its maximum value during the night we can foresee whether the katabatic wind will give rise to a very stable regime or a near-neutral regime within the SBL. In Fig. 10 we characterise the regime transition from relevant non-dimensional numbers by representing V_{TKE} at 4 and 8 m as a measure of turbulence intensity with respect to three nondimensional parameters,

Atmos. Chem. Phys. Discuss., https://doi.org/10.5194/acp-2018-944
Manuscript under review for journal Atmos. Chem. Phys.
Discussion started: 17 October 2018

Atmospheric Chemistry and Physics Discussions

both local and non-local. As stated in Sun et al. (2016), Monin-Obukhov Similarity Theory (MOST) is only applicable in a thin layer above the surface (up to approximately z = 10 m) during SBL conditions. Since our measurements do not exceed that height, we can assume that MOST is complied in the subsequent calculations.

First, we investigate the use of a non-local parameter: the shear capacity (*SC*). It is derived from the *TKE*-budget equation by ignoring the transport and pressure-covariance terms. This dimensionless quantity was first introduced by van Hooijdonk et al. (2015), and it compares the measured shear with the minimum shear required to maintain a continuously turbulent state, which is given by the heat-flux demand (HFD) at the surface. The HFD is calculated from the surface-energy balance as $HFD = R_{net} - G - LH$. *SC* is therefore used to predict the regime transition from the weakly stable boundary layer to the very stable boundary layer, or viceversa. Since turbulence responds to the bulk shear instead of the local shear for a wind speed $U > V_6 =$ 1.5 m s^{-1}, we define the *SC* in this work as:

$$SC(U < 1.5\ m\ s^{-1}) = \left\{ \frac{\rho C_p (\kappa z)^2 \left(\frac{\partial U}{\partial z}\right)^3}{g/\theta_v(z)\ |HFD|} \right\}^{1/3},$$

$$SC(U > 1.5\ m\ s^{-1}) = \left\{ \frac{\rho C_p (\kappa z)^2 \left(\frac{U}{z}\right)^3}{g/\theta_v(z)\ |HFD|} \right\}^{1/3}. \quad (3)$$

θ_v is the virtual potential temperature, κ is the von Kármán constant (=0.4), z is the height agl, $\partial U/\partial z$ is the local shear, U/z the bulk shear, g the gravitational acceleration (9.81 m s^{-2}), ρ is the air density, C_p the specific heat at constant pressure (= 1005 J kg^{-1} K^{-1}) and |HFD| is the absolute value of the HFD at surface, since *SC* is defined only when $\overline{w'\theta'_v} < 0$. $\partial U/\partial z$ was computed by fitting the wind measurements at 3, 6 and 10 m to a log-linear profile as in (1).

van Hooijdonk et al. (2015) observed over flat and homogeneous terrain that independently of the measurement height they could define a *SC* value ($\simeq$ 3) for which the transition from very-stable (low *SC* values) to weakly-stable conditions (higher *SC* values) occurred. In this work we calculate the *SC* at 4 and 8 m (Fig. 10a and b respectively), and we find two transitions (indicated with dashed vertical lines): the first at *SC* = 3 above which both SBL regimes are almost equally found, and the second at *SC* = 4.5, over which the SBL is always weakly stable. The observed transition is independent of height, but we are unable to select a single value for separating the weakly stable and very stable regimes. Instead, the shift between the regimes seems to occur along a transition regime, within which both intense a weak katabatics are observed. The transition is directly related with the HOST hypothesis, given that the *SC* is predominantly dominated by wind shear. As a matter of fact the hockey-stick shaped plot of Fig. 10b resembles Fig. 8b, except that the regime transition is sharper for the *SC*: intense and weak katabatics cluster into two clearly distinct regimes according to the dependence on local or bulk shear. The transition is less sharp at 4 m, since at this level local and bulk shear are closer than at 8 m.

Two other local non-dimensional numbers are investigated: z/L and R_B, being the L the Obukhov length and R_B the bulk Richardson number (Stull, 1988). They are frequently employed in the literature as stability parameters and turbulence-production indicators, with local significance. As occurs for the *SC*, when representing V_{TKE} versus z/L and R_B at 4 and 8 m the transition occurs over a range of values. This transition region was also observed by Mahrt (1998). He found at 10 m that z/L = 0.065 is the limit for the weakly stable boundary layer and z/L = 1 for the very stable boundary layer. We set

respectively these values at 0.05 and 0.25 at 4 m (Fig. 10c), and 0.1 and 0.5 at 8 m (Fig. 10d), the latter coinciding with the value found by Högström (1996). This threshold appears to be very strong, since above it no intense katabatics are found. The regime transition is fuzzier for R_B, in particular the threshold for the weakly stable regime is difficultly identified (Figs. 10e and f). However, it should be taken into account that by definition this nondimensional parameter estimates wind shear from finite differences in height. It does not consider whether wind shear is produced by bulk or local shear, and it will be closer from one or the other depending on the vertical-level separation. In any case, we find that at $\sim R_B = 0.3$–0.35 turbulence production has decayed so that the very stable regime is established, between the measured critical values for the gradient Richardson number $Ri_c = 0.25$ and bulk Richardson number $R_B = 0.5$ (Stull, 1988). Among the three nondimensional parameters, SC seems to be the sharpest and most adequate in foreseeing the regime transition.

5 Analysis of representative katabatic events

So far we have explored all the selected katabatic events together, and learnt about their main characteristics and connection with the SBL regimes. However, in order to better understand the mechanism behind the complex interaction between the katabatic flow and turbulence in the SBL, we target the analysis of individual events.

5.1 Inspecting individual events

We choose a weak and an intense event, so that their contrasting features are revealed. The weak event is August 13 and shows the presence of a skin flow and a very stable SBL regime. In short, the synoptic situation was marked by the Azores high and a thermal low over the Iberian Peninsula inducing a weak S flow, which was related with a weaker katabatic intensity (Fig. 6). The intense event is July 27, and this day the synoptic situation was also characterised by the Azores high, but in this case with a weak NW forcing, associated with greater katabatic intensity. In addition to the strong turbulence associated with the intense katabatic flow, it is chosen due to its particular influence on the CO_2 transport, which is addressed in Sect. 5.2.

To determine how turbulence in the surface layer responds to both katabatic events, we start our analysis showing u_* in Fig. 11a. The onset of the intense katabatic takes place around 1640 UTC during the afternoon transition of the ABL. After this time, u_* continues increasing slowly up to 0.5–0.6 m s^{-1} at 8 m when the SBL is already developed at around 2000–2100 UTC, and even up to 0.9 m s^{-1} later, exceeding the value associated with the diurnal peak. For the weak event the values of u_* at around 1600–1700 UTC are similar to the intense event, but by the time the katabatic flows arrives (at 1830 UTC, coinciding with the moment at which R_{net} turns negative), u_* has already decreased down to 0.1–0.15 m s^{-1}. Except for some sporadic bursts at 8 m, probably induced by isolated top-down turbulence turbulent events, u_* is maintained below 0.1 m s^{-1}, revealing the presence of the very stable regime.

Vertical profiles of U and θ_v are shown below (Figs. 11 (b-g)) at three relevant stages: at the moment of the katabatic onset, when R_{net} turns negative and finally at 2100 UTC when the SBL is well formed. The logarithmic fitting of the discrete observed profiles for both variables and the measurements are shown. As stated in previous sections, intense katabatics arrive earlier in La Herrería when the stratification is still unstable, which is clearly inferred from Fig. 11c. In contrast, the weak katabatic

Atmos. Chem. Phys. Discuss., https://doi.org/10.5194/acp-2018-944
Manuscript under review for journal Atmos. Chem. Phys.
Discussion started: 17 October 2018

Atmospheric Chemistry and Physics Discussions

arrives when R_{net} turns negative and the stratification is already stable. The wind profile for the weak event at the moment of the onset shows a low-level jet below 3 m associated with a skin flow (U < 1 m s^{-1}), while U is stronger and increases linearly with height between 3 and 10 m for the intense event. U continues increasing in the intense event, exceeding 2 m s^{-1} at 6 m when R_{net} turns negative and 3 m s^{-1} at 2100 UTC. This intensification of the katabatic flow shows a different pattern from for instance Grachev et al. (2016). Based on observations from the MATERHORN field campaign, they reported that the wind profile is stationary in time during the katabatic flow. By the time R_{net} < 0, as a consequence of the flow intensification, the layer between 3 and 10 m is well mixed ($\Delta\theta_v \simeq 0$) despite the surface is already cooling down ($\theta_s < \theta_3$). On the contrary, U keeps below 1 m s^{-1} throughout the entire weak katabatic event, and the stable stratification sharpens progressively (for instance $\Delta\theta_v(10-3) \simeq 2$ K at 2100 UTC).

In order to shed more light on the possible factors inducing such a behaviour of the lower SBL in both cases, we explore the time-evolution of the measured shear at 4 and 8 m, $\Delta\theta_v$ and the surface energy balance for the weak and intense katabatic event in Fig. 12. When the onset of the weak katabatic flow takes place wind shear is weak (< 0.1 s^{-1}), $\Delta\theta_v$ > 0 and the heat fluxes (H+LH+G) are unable to balance the radiative loss. As a consequence of the negative imbalance, the surface-based thermal inversion intensifies (up to 2 K) limiting the increase of wind shear: it is mostly below 0.05 s^{-1} after the onset at 4 m. The limitation of wind shear confines H (see the low values in Fig. 9), intensifying the thermal inversion in turn and producing a positive feedback in which the very stable regime is set up. For the intense katabatic, however, the onset takes place when $\Delta\theta_v$ < 0 and $R_{net} \simeq 200$ W m^{-2}. Wind shear increases particularly at 8 m, without being limited by the stable stratification. By the time R_{net} turns negative slightly before 1900 UTC, wind shear is already very high ($\simeq 0.5\ s^{-1}$) and due to the turbulent mixing, $\Delta\theta_v$ is maintained always below 0.2–0.3 K. In fact, 2–3 hours after the onset the heat fluxes balance the radiative loss and the thermal gradient is almost completely destroyed between 3 and 10 m, limiting the thermal inversion to a thin layer close to the surface (below 3 m). This indicates the presence of near-neutral conditions and the set up of the weakly stable regime.

5.2 Impact of katabatic flows and turbulence on CO_2

We finally explore the role of the transport produced by the katabatic flow and the associated different turbulent patterns within the SBL in a relevant scalar: the CO_2. The mixing ratio of CO_2 and the vertical turbulent fluxes are represented in Fig. 13 for the weak and intense katabatic events. The CO_2 mixing ratio is normalised with respect to the daily mean. By so doing, we aim to reduce the uncertainty due to possible biases. In Fig. 13b the measured turbulent fluxes at 4 and 8 m, and the estimated soil respiration flux (R_s) are represented. Since the soil respiration is an important CO_2 source term near the surface, we decided to include it in the analysis. It has been calculated following Lloyd and Taylor (1994) and Jacobs et al. (2007a):

$$R_s = R_{10}\Big(1 - f(SM)\Big)\left(exp\left(\frac{E_0}{283.15R^*}\right)\left(1 - \frac{283.15}{T_s + 273.15}\right)\right), \quad (4)$$

where R* = 8.31·10^{-3} kJ K mol^{-1} is the universal gas constant, E_0 is the activation energy (we employ a value of 53.30 kJ mol^{-1}) and T_s is the soil temperature which has been estimated from the upward longwave radiation. R_{10} is the reference soil-respiration value at 10° C under no water-stress condition, and it can vary significantly from site to site (Jacobs et al., 2007b); in this case, we consider a value of R_{10} = 0.10±0.02 mg m^{-2} s^{-1} given the dry-soil conditions. Finally, (1 - $f(SM)$) is a water-stress

Atmos. Chem. Phys. Discuss., https://doi.org/10.5194/acp-2018-944
Manuscript under review for journal Atmos. Chem. Phys.
Discussion started: 17 October 2018

correction (Jacobs et al., 2007a) where:

$$f(SM) = C\frac{SM_{max}}{SM + SM_{min}}, \tag{5}$$

with C(=0.0016) being a constant, and *SM* the observed soil moisture at 4-cm depth. SM_{max} and SM_{min} are the respective recorded maximum (= 0.14 m^3 m^{-3}) and minimum (= 0.01 m^3 m^{-3}) soil-moisture values throughout the summer.

The normalised CO_2 mixing ratio at 4 and 8 m for the weak and intense events has the same values at 1600 UTC before the surface thermal inversion is set up. It is therefore of great interest comparing these particular weak and intense events having the same initial mixing ratios but contrasting subsequent dynamical and stability conditions. On the weak event the CO_2 starts increasing at around 1730 UTC when the turbulent fluxes at 4 an 8 become positive. Slightly after the onset, which coincides with the set up of the SBL as reported in Sect. 5.1, the CO_2 starts to accumulate close to the surface until 2000 UTC approximately, due to the dominance of the soil flux over photosynthesis and dynamic transport. Later on, the balance between the divergence of the turbulent fluxes and the horizontal and transport explains the variability of the scalar.

The CO_2 for the intense katabatic shows a contrasting evolution. The onset occurs almost 2 hours before, and the diurnal positive vertical CO_2 gradient is reduced beforehand. Due to strong turbulence, the vertical CO_2 fluxes reach values of up 0.2–0.3 mg m^{-2} s^{-1} slightly after the establishment of the SBL (see Fig. 11) at around 1900 UTC, following closely the estimated values of the soil respiration. From that moment and until 2200 UTC, the vertical gradient of the CO_2 is almost null, but the concentration increases around 6 ppm at both levels (note that it cannot be inferred from the normalised concentration in Fig. 13a). Considering in addition that the divergence of the vertical fluxes is mostly positive in that time range ($(\overline{w'CO_2'})_{8m} > (\overline{w'CO_2'})_{4m}$), the increase of the CO_2 concentration is explained by the non-local horizontal transport associated with the intense katabatic flow. From the null vertical gradient of CO_2 between 4 and 8 m and of θ_v between 3 and 10 m (see Fig. 11g), we can assume that the layer between 4 and 8 is well mixed, and since *w* close to the ground is nearly 0 vertical advection can be neglected. From this assumption we can additionally infer the horizontal transport in that layer between 1900 UTC and 2200 UTC following the methodology from Casso-Torralba et al. (2008) based on well-mixed layers.

We based our analysis on the one-dimensional governing equation for CO_2 in between 4 and 8 m. We therefore neglected the effects of soil CO_2. In short, after applying the Reynolds decomposition and averaging of the velocity fluctuations, and by considering the continuity equation we get Eq. 6 for the average CO_2 in the layer between 4 and 8 m. The wind has been aligned in the main component. We additionally neglect the horizontal turbulent flux divergence, since under near-neutral conditions the flux-fetch condition in the katabatic direction is met in our emplacement.

$$\frac{\partial\overline{CO_2}}{\partial t} + \overline{u}\frac{\partial\overline{CO_2}}{\partial x} + \frac{\partial\overline{w'CO_2'}}{\partial z} = 0. \tag{6}$$

The first term represents the storage, the second advection and the third the divergence of the turbulent fluxes in the layer between 4 and 8 m. Since the layer is well mixed, we assume linearity of the turbulent fluxes with height (Casso-Torralba et al. 2008). For the sake of simplicity we consider that the advective term is maintained constant from 1900 to 2200. Integrating

Atmos. Chem. Phys. Discuss., https://doi.org/10.5194/acp-2018-944
Manuscript under review for journal Atmos. Chem. Phys.
Discussion started: 17 October 2018

Atmospheric Chemistry and Physics Discussions

Eq. 6 in time we get to the following equivalence for the horizontal-transport term:

$$\int_{1900}^{2200} \overline{u}\frac{\partial[\overline{CO_2}]}{\partial x}dt = -\int_{1900}^{2200} \frac{\partial[\overline{CO_2}]}{\partial t} - \int_{1900}^{2200} \frac{\Delta\overline{w'CO_2'}}{\Delta z}dt \quad (7)$$

The time evolution of the three terms in shown in Fig. 14, together with the katabatic speed evolution. Since the horizontal gradient of the CO_2 concentration increases upwind of the katabatic flow, the sign of the advective term is negative (note that it is represented in absolute values). After the corresponding calculations in Eq. 7, we obtain that a horizontal transport of 67 ppm over 3 h induced by the intense katabatic flow compensates the loss due to the vertical divergence (around 61 ppm in 3 h), resulting in an increase of the CO_2 storage of 6 ppm. This positive CO_2 advection is probably induced by the presence upwind of a land use composed of forest, mosaic trees and shrubs towards the katabatic direction, which accumulates greater CO_2 concentrations close to the surface during the night due to increased plant respiration and soil flux. Intense katabatics, as demonstrated in previous sections, induce strong wind shear and considerable mixing of the lower SBL, which together with the strong flow, contribute to cause important transport of scalars such as the CO_2.

6 Summary and conclusions

Forty katabatic events of different intensities and with contrasting impacts on the turbulent characteristics of the SBL and on the CO_2 transport and mixing were investigated. Measurements were carried out in a relatively flat area with a relatively dessicated soil at the foothill of a high mountain range in central Spain during one summer. Observations of energy fluxes (heat and momentum), CO_2 and other meteorological variables were recorded in a tower at various vertical levels up to 10 m. A systematic algorithm was employed in order to select unambiguously thermally-driven downslope winds, by using objective filters to account for large-scale and local forcings.

The selected katabatic events were classified into three groups according to the observed maximum katabatic intensity until midnight: weak, moderate and intense. By clustering them into these three groups, we were able to analyse the factors that produce different intensities, and their relationship with the different turbulent patterns in the SBL.

Weak katabatics form when the maximum wind speed is kept below 1.5 m s^{-1}. They particularly take place when the large-scale wind opposes the katabatic flow and soil moisture is greater than the summer median, which in general induces a smaller radiative cooling. These factors give rise to a delayed arrival of the katabatic flow, when the stratification is already neutral or stable, which limits the increase of the wind shear. A positive feedback between the weak turbulence and the progressive cooling of the surface, which induces a more stable stratification, explains the formation of the very stable regime. A skin flow below 3 m and intermittent but weak turbulence are sporadically observed.

Intense katabatics are found when the maximum wind speed exceeds 3.5 m s^{-1} at 6 m agl. They mostly occur when soil moisture is lower than the summer median, the large-scale wind blows in the katabatic direction and its speed is greater than 3.5 m s^{-1} at 850 hPa. These factors induce an earlier katabatic onset, when the stratification is still unstable. Wind shear can

therefore increase without being damped by the stable stratification. By the time the SBL is formed, wind shear is considerably high (up to 0.5 s^{-1}), and the layer between 3 and 10 m is maintained well mixed. Given the strong turbulence, the downward heat flux is finally able to compensate the radiative cooling at the surface, and therefore the thermal inversion is limited to a very thin layer close to the surface. In this way, near-neutral conditions are reached and the weakly stable boundary layer is established.

Moderate katabatics lie between weak and intense katabatics, and their impact on the SBL regime and the associated turbulence is not so clearly assessed. Among all the moderate ones, the weakest events mostly approach the weak katabatics and the strongest events the intense katabatics, although the boundary for the transition between the regimes in this case in unclear.

Our findings show that the regime transition in the SBL is defined by using various values of dimensionless parameters. Instead, it occurs over a certain transitional range which depends on the observational height for z/L and R_B, and is independent of that height in the case of the shear capacity. The latter is the best in predicting the regime transition, as long as the HOST transition is taken into consideration for the corresponding wind-speed threshold. We found, indeed, that the wind speed is the most precise variable for representing the regime transition: above a wind speed of 1.5 m s^{-1} at 6 m, it is the bulk shear which dominates the turbulence production, and the thermal inversion is eroded significantly, giving rise to a regime transition.

Finally we inspected individual intense and a weak katabatic events, and their contribution to the CO_2 budget. On the weak event, the slight turbulence contributes to the accumulation of CO_2 close to the surface, and its concentration is sensitive to slight changes in the turbulent fluxes. For the intense event, instead, turbulence is considerably greater and consequently the layer between 4 and 8 m is well mixed. Under these conditions, we estimated the contribution of the horizontal transport in the katabatic direction, which is of around 67 ppm in 3 h, contributing to the increase in storage of this scalar.

To sum up, we have been able to characterise the evening transition and foresee the turbulent characteristics of the SBL during the night by measuring the maximum intensity of the katabatic flow, which depends on external factors such as the large-scale wind and soil moisture. In particular, the influence of the latter in the surface-energy balance needs further investigation. Being able to predict these external factors more precisely is therefore of high interest to better forecast the night-time turbulence and regime transition. However, sudden turbulent bursts and collapses, and the interaction with gravity waves have not been explored in this work, which can also be relevant in producing perturbations in the SBL and regime transitions. Future studies should tackle with those features and a better performance of numerical models in reproducing them.

Data availability. Original data are freely available upon request through the GuMNet web: https://www.ucm.es/gumnet/

Author contributions. CY, CRC, GM, JAA and MS assisted with the obtention and validation of the quality data, CY lead the project and conducted the field experiment, CRC and MS contributed to the data treatment, JAA carried out the calculations and wrote the manuscript and JVA contributed to the analysis and interpretation of results. All the authors commented on the manuscript.

Competing interests. We declare that not competing interests are present

Acknowledgements. This research has been funded by ATMOUNT-II project [Ref. CGL2015-65627-C3-3-R (MINECO/FEDER)] and the Project [Ref. CGL2016-81828-REDT/AEI] from the Spanish Government, and by the GuMNet (Guadarrama Monitoring Network, www.ucm.es/gumnet) observational network of CEI Moncloa campus of International Excellence. Jon A. Arrillaga is supported by the Predoctoral Training Program for No-Doctor Researchers of the Department of Education, Language Policy and Culture of the Basque Government (PRE_2017_2_0069, MOD = B). We thank the contribution of all the members of the GuMNet Team, especially Dr. J.F. González-Rouco, and *Patrimonio Nacional* for the facilities given during the installation of the meteorological tower.

References

AEMET: Summary of Summer 2017, Spanish Meteorological Agency, http://www.aemet.es/en/noticias/2017/09/Verano_2017, 2017.

Arrillaga, J. A., Yagüe, C., Sastre, M., Román-Cascón, C., Maqueda, G., Inclán, R., González-Roúco, J., Santolaria, E., Durán, L., and Navarro., J.: WRF simulations of upslope and downslope flows over the Guadarrama Mountain Range (Spain), in: 32nd Conference on Agricultural and Forest Meteorology, Salt Lake City (UT, USA), 2016.

Arrillaga, J. A., Vilà-Guerau de Arellano, J., Bosveld, F., Baltink, H. K., Yagüe, C., Sastre, M., and Román-Cascón, C.: Impacts of afternoon and evening sea-breeze fronts on local turbulence, and on CO2 and radon-222 transport, Quart. J. Roy. Meteor. Soc., pp. 1–22, https://doi.org/10.1002/qj.3252, 2018.

Atkinson, B.: Meso-Scale Atmospheric Circulations, Academic Press, London, 1981.

Banta, R. M. and Gannon, P. T.: Influence of soil moisture on simulations of katabatic flow, Theor. Appl. Climatol., 52, 85–94, https://doi.org/10.1007/BF00865509, 1995.

Barry, R. G.: Mountain Weather and Climate, Cambridge University Press, Cambridge, UK., Meteorol. Appl., 17, 506 pp., https://doi.org/10.1002/met.222, 2008.

Borge, R., Narros, A., Artíñano, B., Yagüe, C., Gómez-Moreno, F. J., de la Paz, D., Román-Cascón, C., Díaz, E., Maqueda, G., Sastre, M., Quaassdorff, C., Dimitroulopoulou, C., and Vardoulakis, S.: Assessment of microscale spatio-temporal variation of air pollution at an urban hotspot in Madrid (Spain) through an extensive field campaign, Atmos. Environ., 140, 432 – 445, https://doi.org/https://doi.org/10.1016/j.atmosenv.2016.06.020, 2016.

Borge, R., Artíñano, B., Yagüe, C., Gomez-Moreno, F. J., Saiz-Lopez, A., Sastre, M., Narros, A., García-Nieto, D., Benavent, N., Maqueda, G., Barreiro, M., de Andrés, J. M., and Ángeles Cristóbal: Application of a short term air quality action plan in Madrid (Spain) under a high-pollution episode - Part I: Diagnostic and analysis from observations, Sci Total Environ, 635, 1561 – 1573, https://doi.org/https://doi.org/10.1016/j.scitotenv.2018.03.149, 2018.

Casso-Torralba, P., Vilà-Guerau de Arellano, J., Bosveld, F., Soler, M. R., Vermeulen, A., Werner, C., and Moors, E.: Diurnal and vertical variability of the sensible heat and carbon dioxide budgets in the atmospheric surface layer, J. Geophys. Res. Atmos., 113, n/a–n/a, https://doi.org/10.1029/2007JD009583, d12119, 2008.

Cristofanelli, P., Calzolari, F., Bonafè, U., Lanconelli, C., Lupi, A., Busetto, M., Vitale, V., Colombo, T., and Bonasoni, P.: Five-year analysis of background carbon dioxide and ozone variations during summer seasons at the Mario Zucchelli station (Antarctica), Tellus B, 63, 831–842, https://doi.org/10.1111/j.1600-0889.2011.00576.x, 2011.

Doran, J. C.: The effects of ambient winds on valley drainage flows, Boundary Layer Meteorol., 55, 177–189, https://doi.org/10.1007/BF00119333, 1991.

Durán, L., Sánchez, E., and Yagüe, C.: Climatology of precipitation over the Iberian Central System mountain range, Int. J. Climatol., 33, 2260–2273, https://doi.org/10.1002/joc.3602, 2013.

Durán, L., I., R.-M., and Sánchez, E.: The Peñalara Mountain Meteorological Network (1999–2014): Description, Preliminary Results and Lessons Learned, Atmosphere, 8, 203, https://doi.org/https://doi.org/10.3390/atmos8100203, 2018.

Fitzjarrald, D. R.: Katabatic Wind in Opposing Flow, J. Atmos. Sci., 41, 1143–1158, https://doi.org/10.1175/1520-0469(1984)041<1143:KWIOF>2.0.CO;2, 1984.

Grachev, A. A., Leo, L. S., Sabatino, S. D., Fernando, H. J. S., Pardyjak, E. R., and Fairall, C. W.: Structure of Turbulence in Katabatic Flows Below and Above the Wind-Speed Maximum, Boundary Layer Meteorol., 159, 469–494, https://doi.org/10.1007/s10546-015-0034-8, 2016.

GuMNet: www.ucm.es/gumnet/, www.ucm.es/gumnet/, 2018.

Hang, C., Nadeau, D. F., Gultepe, I., Hoch, S. W., Román-Cascón, C., Pryor, K., Fernando, H. J. S., Creegan, E. D., Leo, L. S., Silver, Z., and Pardyjak, E. R.: A Case Study of the Mechanisms Modulating the Evolution of Valley Fog, Pure Appl. Geophys., 173, 3011–3030, https://doi.org/10.1007/s00024-016-1370-4, 2016.

Högström, U.: Review of some basic characteristics of the atmospheric surface layer, Boundary Layer Meteorol., 78, 215–246, https://doi.org/10.1007/BF00120937, 1996.

Horst, T. W. and Doran, J. C.: Nocturnal drainage flow on simple slopes, Boundary Layer Meteorol., 34, 263–286, https://doi.org/10.1007/BF00122382, 1986.

Jacobs, A. F. G., Heusinkveld, B. G., and Holtslag, A. A. M.: Seasonal and interannual variability of carbon dioxide and water balances of a grassland, Clim. Change, 82, 163–177, https://doi.org/https://doi.org/10.1007/s10584-006-9182-7, 2007a.

Jacobs, C. M. J., Jacobs, A. F. G., Bosveld, F. C., Hendriks, D. M. D., Hensen, A., Kroon, P. S., Moors, E. J., Nol, L., Schrier-Uijl, A., and Veenendaal, E. M.: Variability of annual CO_2 exchange from Dutch grasslands, Biogeosciences, 4, 803–816, https://doi.org/10.5194/bg-4-803-2007, 2007b.

Jensen, D., Nadeau, D. F., Hoch, S. W., and Pardyjak, E. R.: The evolution and sensitivity of katabatic flow dynamics to external influences through the evening transition, Quart. J. Roy. Meteor. Soc., 143, 423–438, https://doi.org/10.1002/qj.2932, 2017.

Legrand, M., Preunkert, S., Savarino, J., Frey, M. M., Kukui, A., Helmig, D., Jourdain, B., Jones, A. E., Weller, R., Brough, N., and Gallée, H.: Inter-annual variability of surface ozone at coastal (Dumont d'Urville, 2004–2014) and inland (Concordia, 2007–2014) sites in East Antarctica, Atmos. Chem. Phys., 16, 8053–8069, https://doi.org/10.5194/acp-16-8053-2016, 2016.

Lehner, M., Whiteman, C. D., Hoch, S. W., Jensen, D., Pardyjak, E. R., Leo, L. S., Di Sabatino, S., and Fernando, H. J. S.: A Case Study of the Nocturnal Boundary Layer Evolution on a Slope at the Foot of a Desert Mountain, J. Appl. Meteor. Climatol., 54, 732–751, https://doi.org/10.1175/JAMC-D-14-0223.1, 2015.

Li, J., Sun, J., Zhou, M., Cheng, Z., Li, Q., Cao, X., and Zhang, J.: Observational analyses of dramatic developments of a severe air pollution event in the Beijing area, Atmos. Chem. Phys., 18, 3919–3935, https://doi.org/10.5194/acp-18-3919-2018, 2018.

Lloyd, J. and Taylor, J.: On the Temperature Dependence of Soil Respiration, Funct. Ecol., 8, 315–323, 1994.

Lothon, M., Lohou, F., Pino, D., Couvreux, F., Pardyjak, E. R., Reuder, J., Vilà-Guerau de Arellano, J., Durand, P., Hartogensis, O., Legain, D., Augustin, P., Gioli, B., Lenschow, D. H., Faloona, I., Yagüe, C., Alexander, D. C., Angevine, W. M., Bargain, E., Barrié, J., Bazile, E., Bezombes, Y., Blay-Carreras, E., van de Boer, A., Boichard, J. L., Bourdon, A., Butet, A., Campistron, B., de Coster, O., Cuxart, J., Dabas, A., Darbieu, C., Deboudt, K., Delbarre, H., Derrien, S., Flament, P., Fourmentin, M., Garai, A., Gibert, F., Graf, A., Groebner, J., Guichard, F., Jiménez, M. A., Jonassen, M., van den Kroonenberg, A., Magliulo, V., Martin, S., Martinez, D., Mastrorillo, L., Moene, A. F., Molinos, F., Moulin, E., Pietersen, H. P., Piguet, B., Pique, E., Román-Cascón, C., Rufin-Soler, C., Saïd, F., Sastre-Marugán, M., Seity, Y., Steeneveld, G. J., Toscano, P., Traullé, O., Tzanos, D., Wacker, S., Wildmann, N., and Zaldei, A.: The BLLAST field experiment: Boundary-Layer Late Afternoon and Sunset Turbulence, Atmos. Chem. Phys., 14, 10 931–10 960, https://doi.org/10.5194/acp-14-10931-2014, 2014.

Mahrt, L.: Nocturnal Boundary-Layer Regimes, Boundary Layer Meteorol., 88, 255–278, https://doi.org/10.1023/A:1001171313493, 1998.

Mahrt, L.: Stably Stratified Atmospheric Boundary Layers, Annu. Rev. Fluid Mech., 46, 23–45, https://doi.org/10.1146/annurev-fluid-010313-141354, 2014.

Mahrt, L. and Larsen, S.: Relation of slope winds to the ambient flow over gentle terrain, Boundary Layer Meteorol., 53, 93–102, https://doi.org/10.1007/BF00122465, 1990.

Nadeau, D., Pardyjak, E. R., Higgins, C. W., Huwald, H., and Parlange, M. B.: Flow during the evening transition over steep Alpine slopes, Quart J Roy Meteor Soc, 139, 607–624, 2013.

Oldroyd, H. J., Pardyjak, E. R., Higgins, C. W., and Parlange, M. B.: Buoyant Turbulent Kinetic Energy Production in Steep-Slope Katabatic Flow, Boundary Layer Meteorol., 161, 405–416, https://doi.org/10.1007/s10546-016-0184-3, 2016.

Pardyjak, E. R., Fernando, H., Joseph S. Hunt, J. C. G., and Anderson, J.: A case study of the development of nocturnal slope flows in a wide open valley and associated air quality implications, Meteorol. Z., 18, 85–100, https://doi.org/10.1127/0941-2948/2009/362, 2009.

Plaza, J., Pujadas, M., and Artíñano, B.: Formation and Transport of the Madrid Ozone Plume, J Air Waste Manag Assoc, 47, 766–774, https://doi.org/10.1080/10473289.1997.10463938, 1997.

Poulos, G. and Zhong, S.: An Observational History of Small-Scale Katabatic Winds in Mid-Latitudes, Geogr. Compass, 2, 1798–1821, https://doi.org/10.1111/j.1749-8198.2008.00166.x, 2008.

Poulos, G. S., Blumen, W., Fritts, D. C., Lundquist, J. K., Sun, J., Burns, S. P., Nappo, C., Banta, R., Newsom, R., Cuxart, J., Terradellas, E., Balsley, B., and Jensen, M.: CASES-99: A Comprehensive Investigation of the Stable Nocturnal Boundary Layer, Bull. Amer. Meteor. Soc., 83, 555–582, https://doi.org/10.1175/1520-0477(2002)083<0555:CACIOT>2.3.CO;2, 2002.

Román-Cascón, C., Yagüe, C., Mahrt, L., Sastre, M., Steeneveld, G.-J., Pardyjak, E., van de Boer, A., and Hartogensis, O.: Interactions among drainage flows, gravity waves and turbulence: a BLLAST case study, Atmos. Chem. Phys., 15, 9031–9047, https://doi.org/10.5194/acp-15-9031-2015, 2015.

Rotach, M. W., Wohlfahrt, G., Hansel, A., Reif, M., Wagner, J., and Gohm, A.: The World is Not Flat: Implications for the Global Carbon Balance, Bull. Amer. Meteor. Soc., 95, 1021–1028, https://doi.org/10.1175/BAMS-D-13-00109.1, 2014.

Sastre, M., Yagüe, C., Román-Cascón, C., and Maqueda, G.: Atmospheric Boundary-Layer Evening Transitions: A Comparison Between Two Different Experimental Sites., Boundary-Layer Meteorol., 157, 375 – 399, 2015.

Stiperski, I. and Rotach, M. W.: On the Measurement of Turbulence Over Complex Mountainous Terrain, Boundary-Layer Meteorol., 159, 97–121, https://doi.org/10.1007/s10546-015-0103-z, 2016.

Stull, R. B.: An Introduction to Boundary Layer Meteorology, Kluwer Academic Publishers, 1988.

Sun, H., Clark, T. L., Stull, R. B., and Black, T. A.: Two-dimensional simulation of airflow and carbon dioxide transport over a forested mountain: Part II. Carbon dioxide budget analysis and advection effects, Agric. For. Meteorol., 140, 352 – 364, https://doi.org/https://doi.org/10.1016/j.agrformet.2006.03.016, the Fluxnet-Canada Research Network: Influence of Climate and Disturbance on Carbon Cycling in Forests and Peatlands, 2006.

Sun, J., Burns, S. P., Delany, A. C., Oncley, S. P., Turnipseed, A. A., Stephens, B. B., Lenschow, D. H., LeMone, M. A., Monson, R. K., and Anderson, D. E.: CO2 transport over complex terrain, Agric. For. Meteorol., 145, 1 – 21, https://doi.org/https://doi.org/10.1016/j.agrformet.2007.02.007, 2007.

Sun, J., Mahrt, L., Banta, R. M., and Pichugina, Y. L.: Turbulence Regimes and Turbulence Intermittency in the Stable Boundary Layer during CASES-99, J. Atmos. Sci., 69, 338–351, https://doi.org/10.1175/JAS-D-11-082.1, 2012.

Sun, J., Mahrt, L., Nappo, C., and Lenschow, D. H.: Wind and Temperature Oscillations Generated by Wave–Turbulence Interactions in the Stably Stratified Boundary Layer, J. Atmos. Sci., 72, 1484–1503, https://doi.org/10.1175/JAS-D-14-0129.1, 2015.

Sun, J., Lenschow, D. H., LeMone, M. A., and Mahrt, L.: The Role of Large-Coherent-Eddy Transport in the Atmospheric Surface Layer Based on CASES-99 Observations, Boundary-Layer Meteorol., 160, 83–111, https://doi.org/10.1007/s10546-016-0134-0, 2016.

Terradellas, E. and Cano, D.: Implementation of a Single-Column Model for Fog and Low Cloud Forecasting at Central-Spanish Airports, Pure Appl. Geophys., 164, 1327–1345, 2007.

Van de Wiel, B. J. H., Moene, A. F., Steeneveld, G., Baas, P., Bosveld, F., and Holtslag, A. A. M.: Intermittent Turbulence and Oscillations in the Stable Boundary Layer over Land. Part III: A classification for observations during CASES-99, J. Atmos. Sci., 60, 2509–2522, https://doi.org/10.1175/1520-0469(2002)059<2567:ITAOIT>2.0.CO;2, 2003.

Van de Wiel, B. J. H., Moene, A. F., and Jonker, H. J. J.: The Cessation of Continuous Turbulence as Precursor of the Very Stable Nocturnal Boundary Layer, J. Atmos. Sci., 69, 3097–3115, https://doi.org/10.1175/JAS-D-12-064.1, 2012a.

Van de Wiel, B. J. H., Moene, A. F., Jonker, H. J. J., Baas, P., Basu, S., Donda, J. M. M., Sun, J., and Holtslag, A. A. M.: The Minimum Wind Speed for Sustainable Turbulence in the Nocturnal Boundary Layer, J. Atmos. Sci., 69, 3116–3127, https://doi.org/10.1175/JAS-D-12-0107.1, 2012b.

van der Linden, S. J. A., Baas, P., Antoon van Hooft, J., van Hooijdonk, I. G. S., Bosveld, F. C., and van de Wiel, B. J. H.: Local Characteristics of the Nocturnal Boundary Layer in Response to External Pressure Forcing, J. Appl. Meteor. Climatol., 56, 3035–3047, https://doi.org/10.1175/JAMC-D-17-0011.1, 2017.

van Hooijdonk, I. G. S., Donda, J. M. M., Clercx, H. J. H., Bosveld, F. C., and van de Wiel, B. J. H.: Shear Capacity as Prognostic for Nocturnal Boundary Layer Regimes, J. Atmos. Sci., 72, 1518–1532, https://doi.org/10.1175/JAS-D-14-0140.1, 2015.

Whiteman, C.: Mountain Meteorology: Fundamentals and Applications, Oxford University Press, 2000.

Whiteman, C. D.: Breakup of Temperature Inversions in Deep Mountain Valleys: Part I. Observations, J. Appl. Meteorol., 21, 270–289, https://doi.org/10.1175/1520-0450(1982)021<0270:BOTIID>2.0.CO;2, 1982.

Zardi, D. and Whiteman, C.: Mountain Weather Research and Forecasting: Recent Progress and Current Challenges, vol. XIII of *Springer Atmospheric Sciences*, chap. Diurnal Mountain WInd Systems., pp. 35–119, Springer Netherlands, 1 edn., 2013.

Atmos. Chem. Phys. Discuss., https://doi.org/10.5194/acp-2018-944
Manuscript under review for journal Atmos. Chem. Phys.
Discussion started: 17 October 2018

Atmospheric Chemistry and Physics Discussions

Table 1. Technical specifications about the variables measured and the devices employed in this study over the intensive summer 2017 campaign [22/06–26/09].

Variable	Height (m, agl)	Instrument	Model
Air Temperature*	3, 6, 10	Aspirated thermometer	Young 41342
Wind speed	3, 6, 10	Cup anemometer	Vector A100LK
Wind direction	10	Wind vane	Vector W200P
Turbulent fluxes**	4, 8	IRGASON***	Campbell
Rain	surface	Pluviometer	OTT Pluvio^2
Soil moisture****	-0.04	Reflectometer	CS655
Soil-heat flux	-0.04	Heat-flux plate	Hukseflux HFP01SC
Radiation components	2	4-component radiometer	Hukseflux NR01
CO_2 concentration**	4, 8	IRGASON	Campbell

* The sampling rate of atmospheric non-turbulent variables is of 1 Hz.

** The averaging period of the turbulent fluxes is 10 minutes.

*** The sampling rate of turbulent variables is of 10 Hz.

**** The sampling rate of soil variables is of 10 minutes.

Atmos. Chem. Phys. Discuss., https://doi.org/10.5194/acp-2018-944
Manuscript under review for journal Atmos. Chem. Phys.
Discussion started: 17 October 2018

Atmospheric Chemistry and Physics Discussions

Table 2. Algorithm for katabatic criteria. First column indicates the filter number; second column the physical description of the filter; and third column, the criteria to be fulfilled in order to pass each of the filters.

Filter	Criteria	Description
1	Weak large-scale winds	V_{850} < 6 m s^{-1}
2	Days without synoptic cold fronts	$(\Delta\theta_{e,850}/\Delta t)$ > -1.5 ° C / 6h
3	Non-rainy events	pp < 0.5 mm/day
4	Minimum persistence in the katabatic direction	WD ϵ [250°–340°]$_{2h}$

Atmos. Chem. Phys. Discuss., https://doi.org/10.5194/acp-2018-944
Manuscript under review for journal Atmos. Chem. Phys.
Discussion started: 17 October 2018

Atmospheric Chemistry and Physics Discussions

Table 3. Classification of katabatic types according to their maximum 10-min averaged wind speed at 6 m from the onset until 24 UTC.

Type	Definition
Weak	$U_{max} < 1.5$ m s^{-1}
Moderate	1.5 m s^{-1} $\leq U_{max} \leq$ 3.5 m s^{-1}
Intense	$U_{max} > 3.5$ m s^{-1}

Atmos. Chem. Phys. Discuss., https://doi.org/10.5194/acp-2018-944
Manuscript under review for journal Atmos. Chem. Phys.
Discussion started: 17 October 2018

Atmospheric Chemistry and Physics Discussions

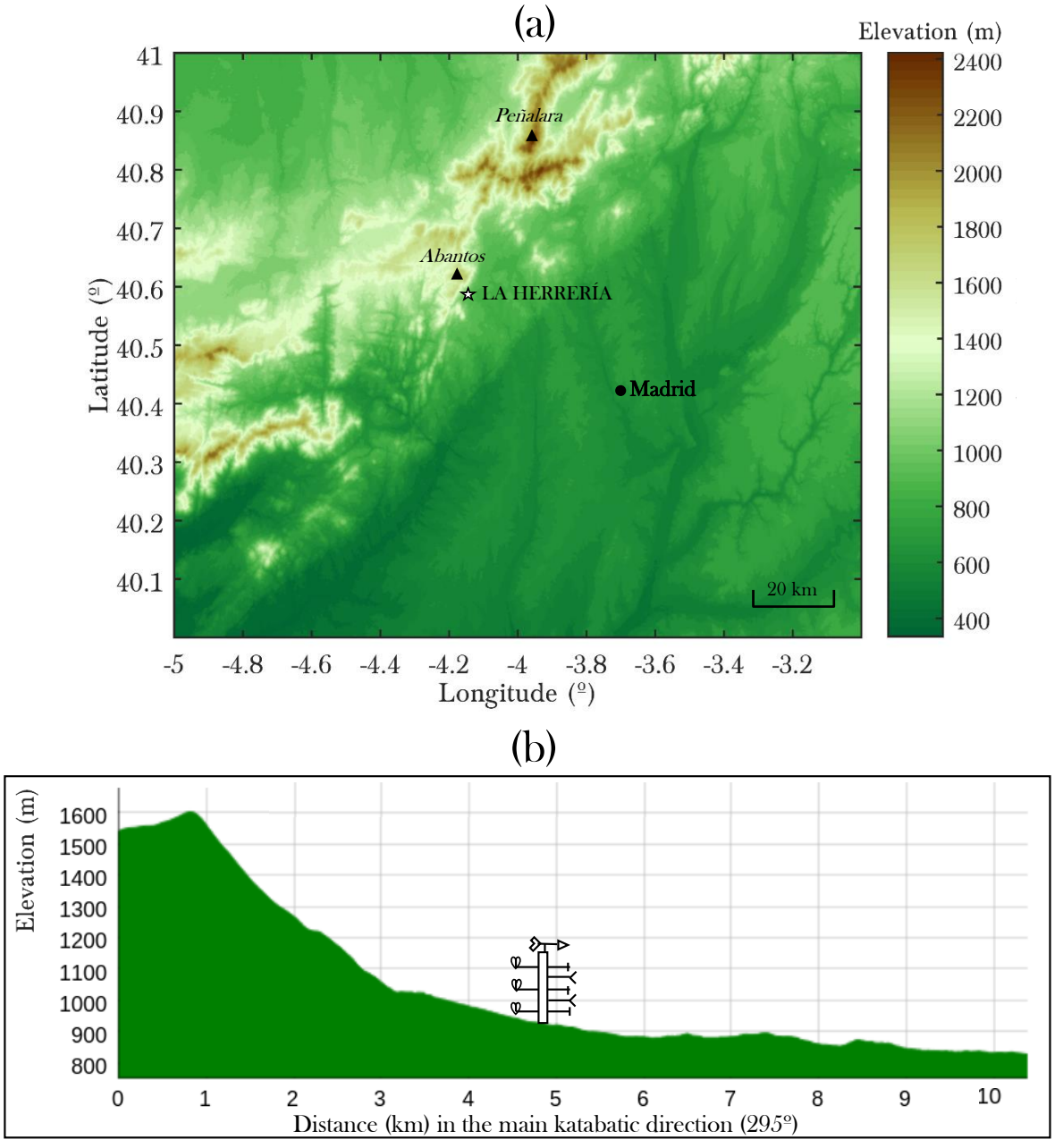

Figure 1. (a) Topography of the area surrounding La Herrería site, which is indicated with a star. Additionally, the position of the city of Madrid, and Abantos (1763 m) and Peñalara peaks (2420 m) are pointed out. The source of topography data is ASTER GDEM, which is a product of NASA and METI. (b) Topographical profile in the main katabatic direction from La Herrería, depicted ∼5 km around in both directions. It is obtained from the *Geocontext-Profiler* tool.

Atmos. Chem. Phys. Discuss., https://doi.org/10.5194/acp-2018-944
Manuscript under review for journal Atmos. Chem. Phys.
Discussion started: 17 October 2018

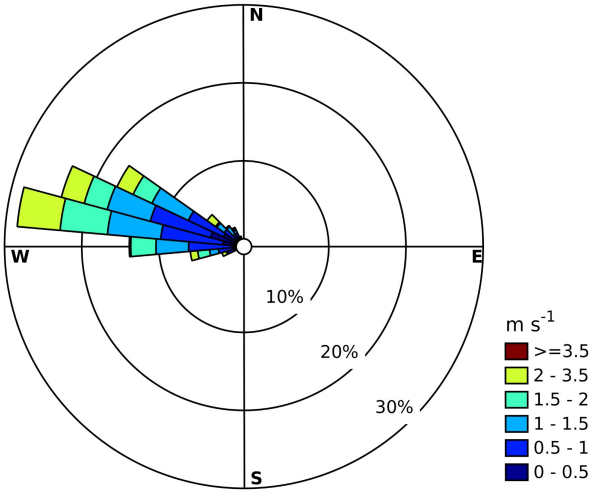

Figure 2. Wind rose at 6 m over the 2 h after the onset of the katabatic flow for the 40 selected events.

Atmos. Chem. Phys. Discuss., https://doi.org/10.5194/acp-2018-944
Manuscript under review for journal Atmos. Chem. Phys.
Discussion started: 17 October 2018

Atmospheric Chemistry and Physics Discussions

(a) Onset

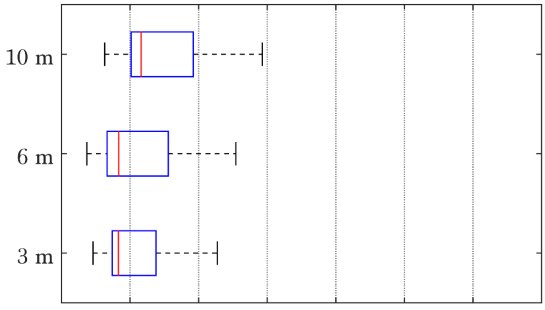

(b) Maximum intensity (considering values at 6 m).

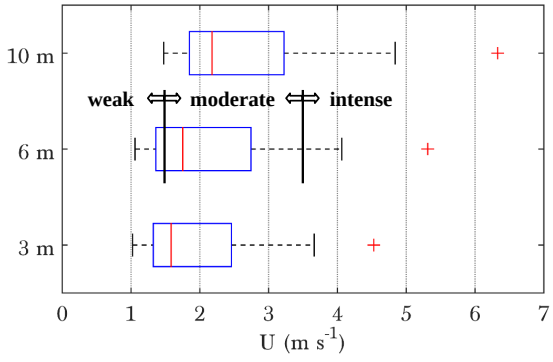

Figure 3. Box plots of the wind speed profile at 3, 6 and 10 m for the katabatic events, (a) at the time of the onset and (b) for the maximum value (from the onset till 2400 UTC) for each level. The red vertical line within blue boxes represents the median, the blue box delimits first and third quartiles, and whiskers delimit the most extreme points not considered outliers (red crosses). Black vertical lines and arrows pinpoint the limits for the wind speed at 6 m that separate weak, moderate and intense of katabatics.

Atmos. Chem. Phys. Discuss., https://doi.org/10.5194/acp-2018-944
Manuscript under review for journal Atmos. Chem. Phys.
Discussion started: 17 October 2018

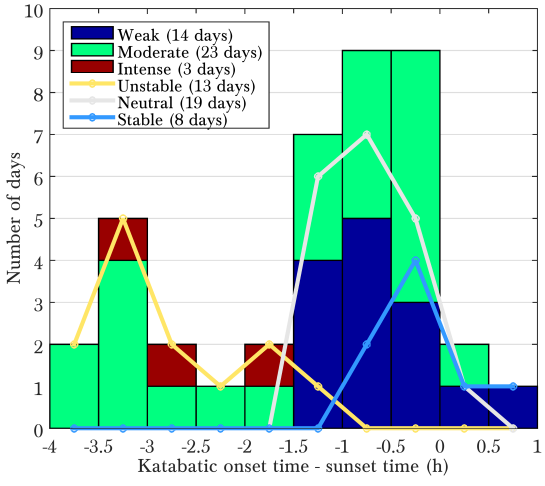

Figure 4. Histograms of the difference between the katabatic onset time and sunset time, for the three groups of intensities (bars) and for different thermal stratification at the moment of the onset (lines).

Atmos. Chem. Phys. Discuss., https://doi.org/10.5194/acp-2018-944
Manuscript under review for journal Atmos. Chem. Phys.
Discussion started: 17 October 2018

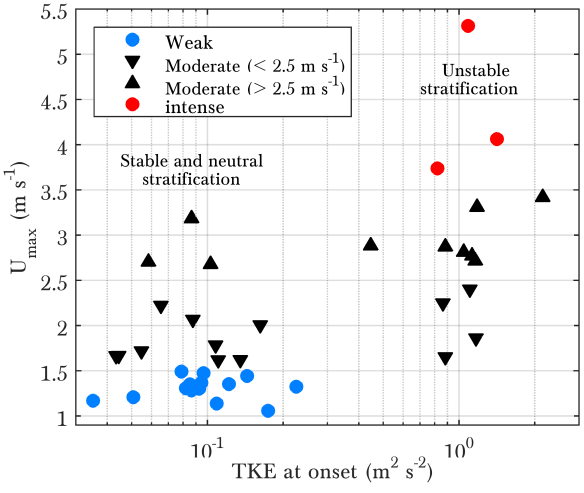

Figure 5. Maximum wind speed (U_{max}) at 6 m for each katabatic event versus TKE at 8 m at the moment of the katabatic onset. Note that the moderate katabatics are divided into two subgroups.

Atmos. Chem. Phys. Discuss., https://doi.org/10.5194/acp-2018-944
Manuscript under review for journal Atmos. Chem. Phys.
Discussion started: 17 October 2018

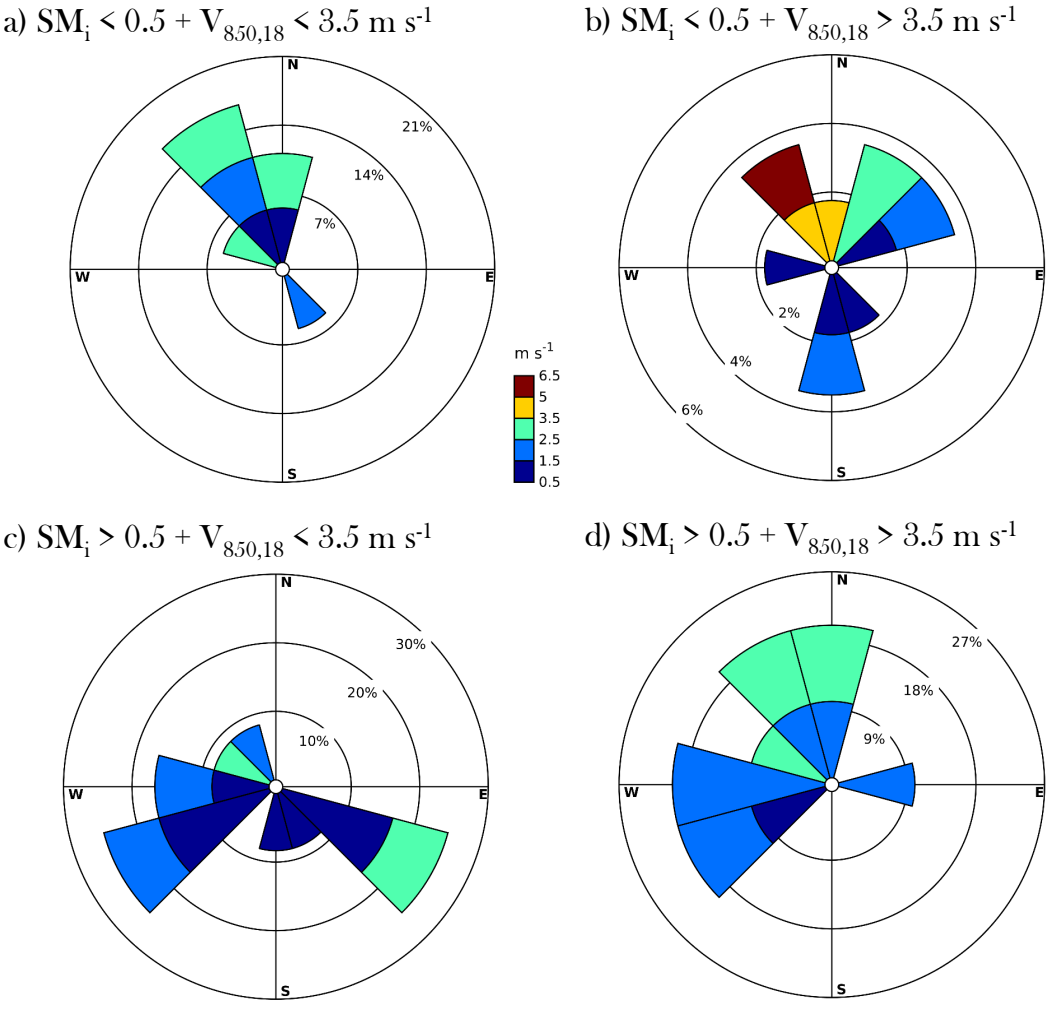

Figure 6. Wind roses representing the maximum katabatic wind speed at 6 m in colours, for different directions from the NCEP-reanalysis wind at 850 hPa, at the closest grid point to La Herrería (40.5° N, 4° W) at 18 UTC. Wind roses are shown for different values of the soil-moisture index (SM_i) and the reanalysis wind speed ($V_{850,18}$) (a-d). Note that the frequency scale of the wind roses is variable.

Atmos. Chem. Phys. Discuss., https://doi.org/10.5194/acp-2018-944
Manuscript under review for journal Atmos. Chem. Phys.
Discussion started: 17 October 2018

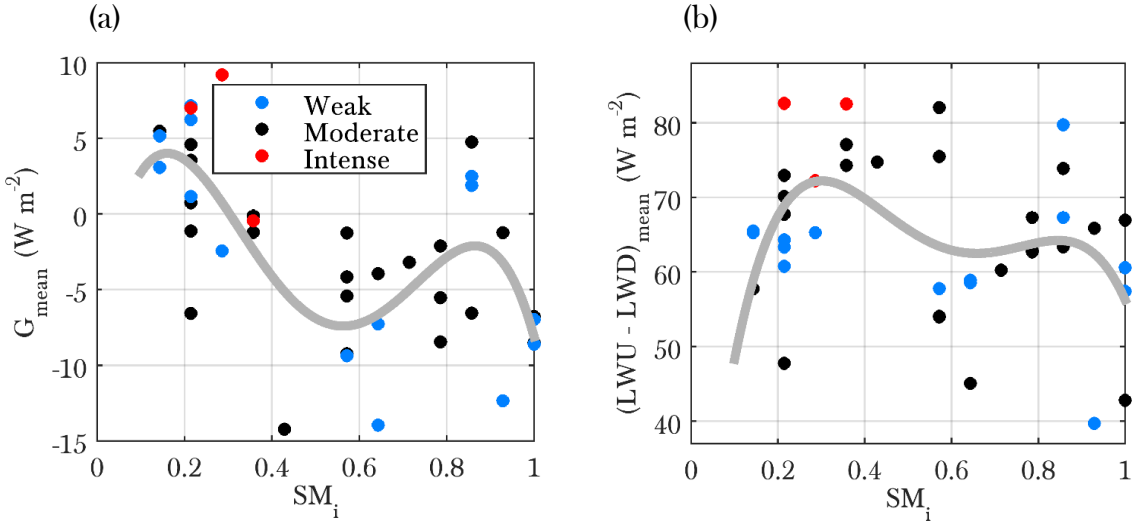

Figure 7. (a) Average soil-heat flux (*G*) and (b) average longwave-radiative loss (*LWU-LWD*) during the katabatic stage (from the onset until 2400 UTC) *vs* the soil-moisture index (SM_i). The grey line represents the 4-th order polynomial fitting of the data.

Atmos. Chem. Phys. Discuss., https://doi.org/10.5194/acp-2018-944
Manuscript under review for journal Atmos. Chem. Phys.
Discussion started: 17 October 2018

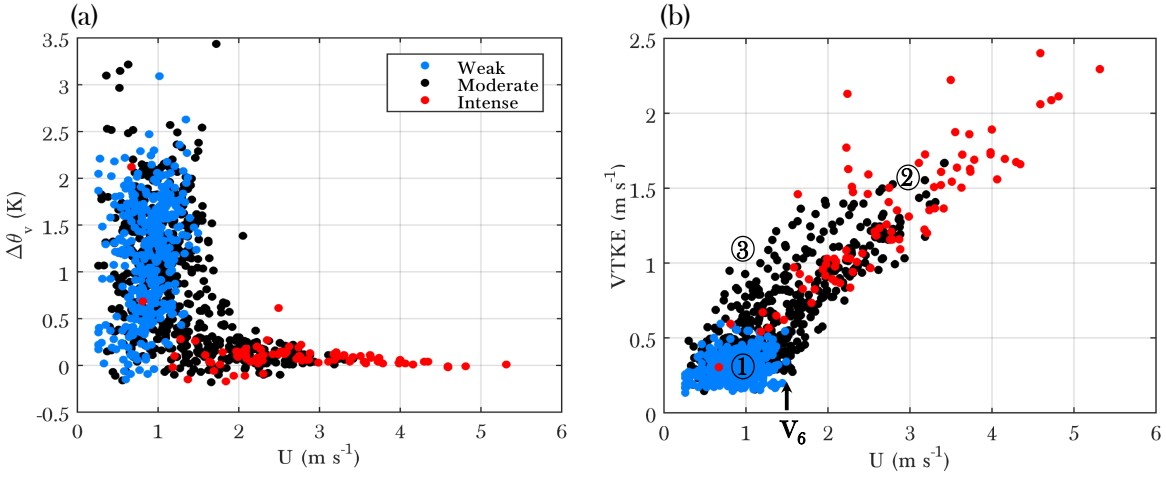

Figure 8. (a) Temperature stratification ($\Delta\theta_v$)and (b) turbulence velocity scale (V_{TKE}) at 8 m versus wind speed (U) at 6 m. The numbers pinpoint the SBL regimes defined in Sun et al. (2012): (1) weak turbulence driven by local instabilities, (2) intense turbulence driven by the bulk shear, and (3) moderate turbulence driven by top-down events. The threshold wind-speed (V_6) at which the HOST transition occurs is indicated too.

Atmos. Chem. Phys. Discuss., https://doi.org/10.5194/acp-2018-944
Manuscript under review for journal Atmos. Chem. Phys.
Discussion started: 17 October 2018

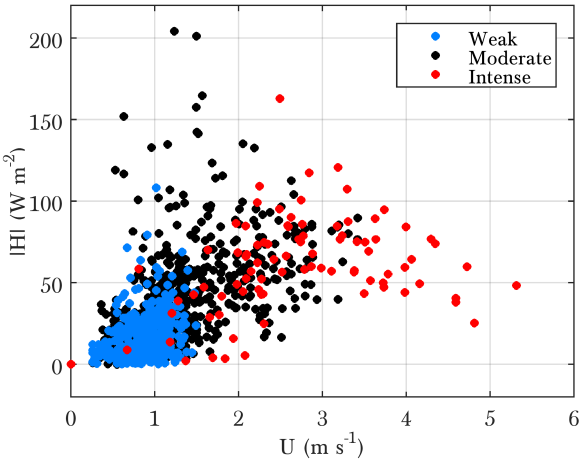

Figure 9. Absolute value of the sensible-heat flux (H) *vs* wind speed (U) at 6 m.

Atmos. Chem. Phys. Discuss., https://doi.org/10.5194/acp-2018-944
Manuscript under review for journal Atmos. Chem. Phys.
Discussion started: 17 October 2018

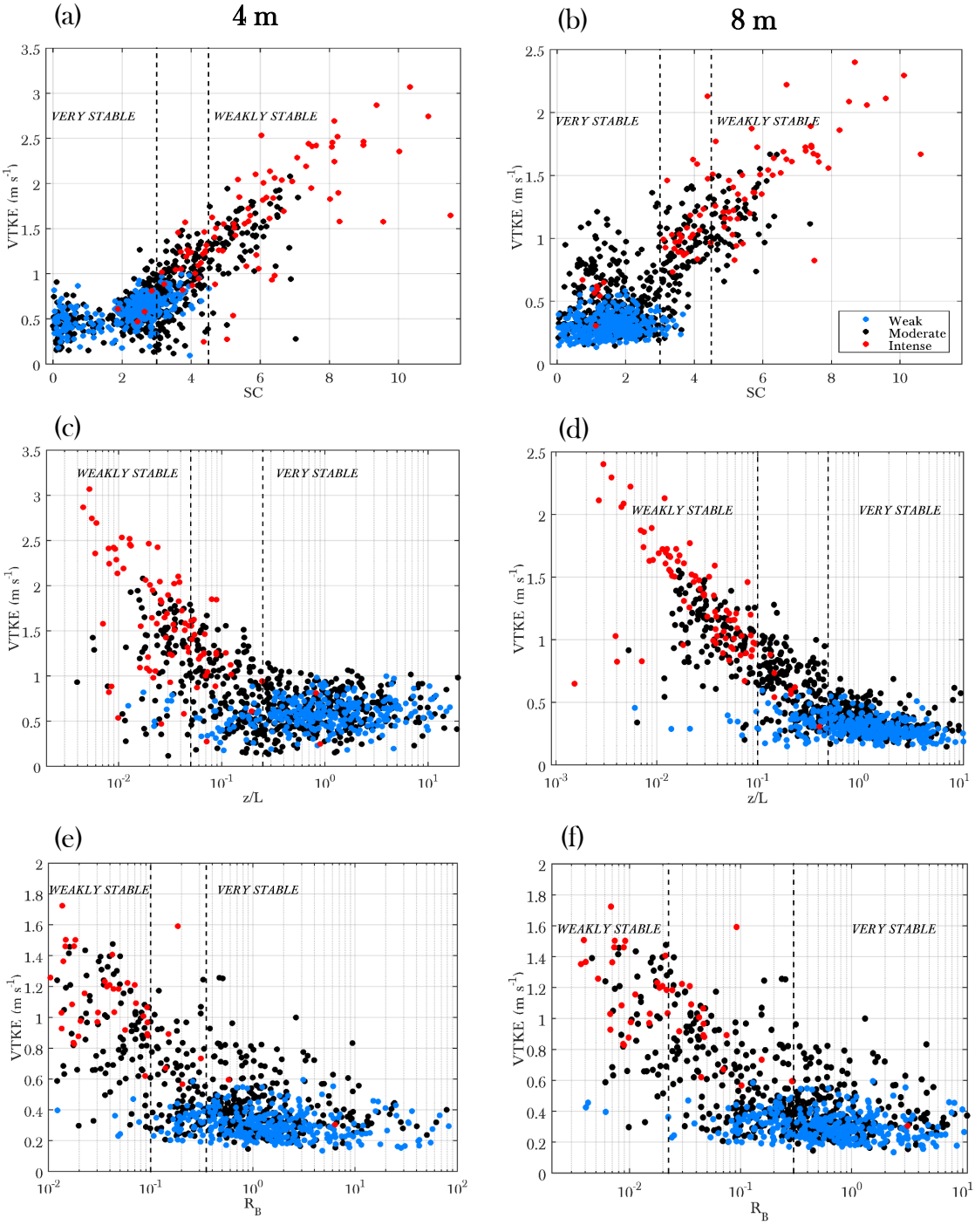

Figure 10. V_{TKE} at z = 4 and 8 m as a function of different non-dimensional parameters: SC (a,b), z/L (c,d) and R_B (e,f). The colour legend is shown in Fig. 8. Vertical dashed lines represent the values of the non-dimensional parameters that delimit the very stable and weakly stable regimes in the SBL.

Atmos. Chem. Phys. Discuss., https://doi.org/10.5194/acp-2018-944
Manuscript under review for journal Atmos. Chem. Phys.
Discussion started: 17 October 2018

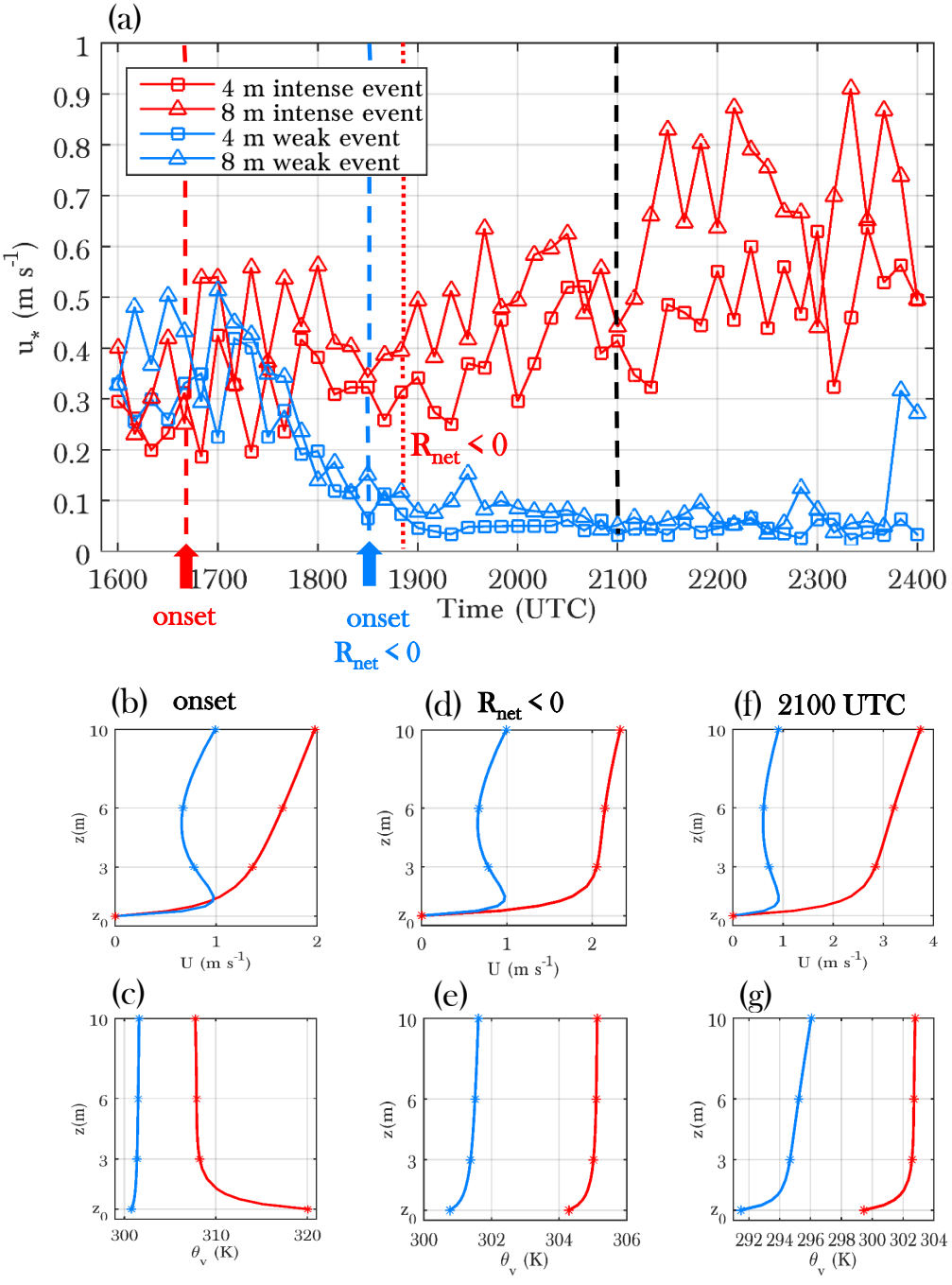

Figure 11. (a) Time evolution of the friction velocity (u_*) at 4 and 8 m for a weak-katabatic (13/08/2017) and an intense-katabatic event (27/07/2017). The coloured arrows and the tied dashed vertical lines indicate the respective onset times, the red pointed line the time at which R_{net} turns negative for the intense event, and the dashed black vertical line is represented at 2100 UTC when the SBL is already well developed for both events. (b-g) Vertical profiles of the wind speed (U) and virtual potential temperature (θ_v) at the onset time (b,c), when R_{net} turns negative (d,e), and at 2100 UTC (f,g). Note that the horizontal scales are variable.

Atmos. Chem. Phys. Discuss., https://doi.org/10.5194/acp-2018-944
Manuscript under review for journal Atmos. Chem. Phys.
Discussion started: 17 October 2018

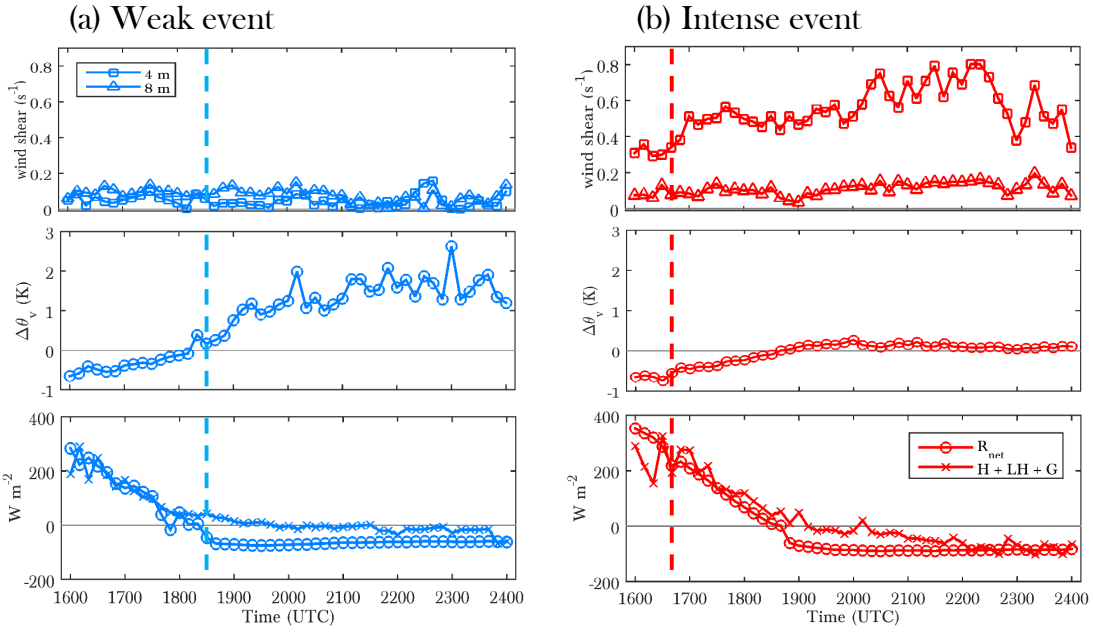

Figure 12. Time evolution of the wind shear at 4 and 8 m, thermal stratification ($\Delta\theta_v$) and the surface-energy balance for the weak (a) and the intense (b) events. The vertical dashed line indicates the onset time of the katabatic flow.

Atmos. Chem. Phys. Discuss., https://doi.org/10.5194/acp-2018-944
Manuscript under review for journal Atmos. Chem. Phys.
Discussion started: 17 October 2018

Atmospheric Chemistry and Physics Discussions

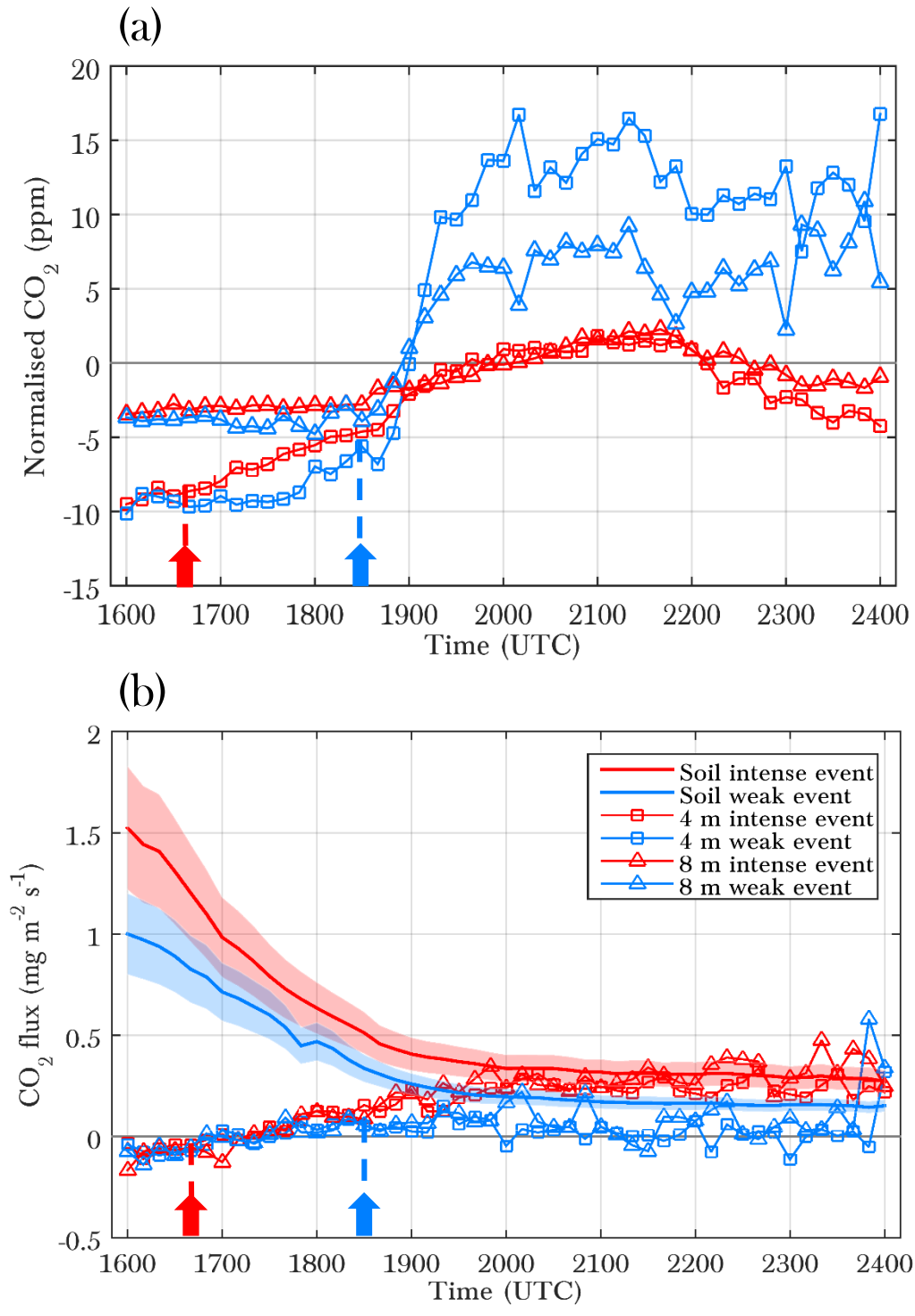

Figure 13. Time evolution of the normalised CO_2 mixing ratio (a) and vertical turbulent fluxes (b) at 4 and 8 m agl for the weak (blue) and intense (red) events. In (b) we include in solid lines the soil-respiration estimation and the 20% uncertainty of R_{10} (see Eq.4) in shaded. The onset of the katabatic flow is indicated from faced arrows of respective colours.

Atmos. Chem. Phys. Discuss., https://doi.org/10.5194/acp-2018-944
Manuscript under review for journal Atmos. Chem. Phys.
Discussion started: 17 October 2018

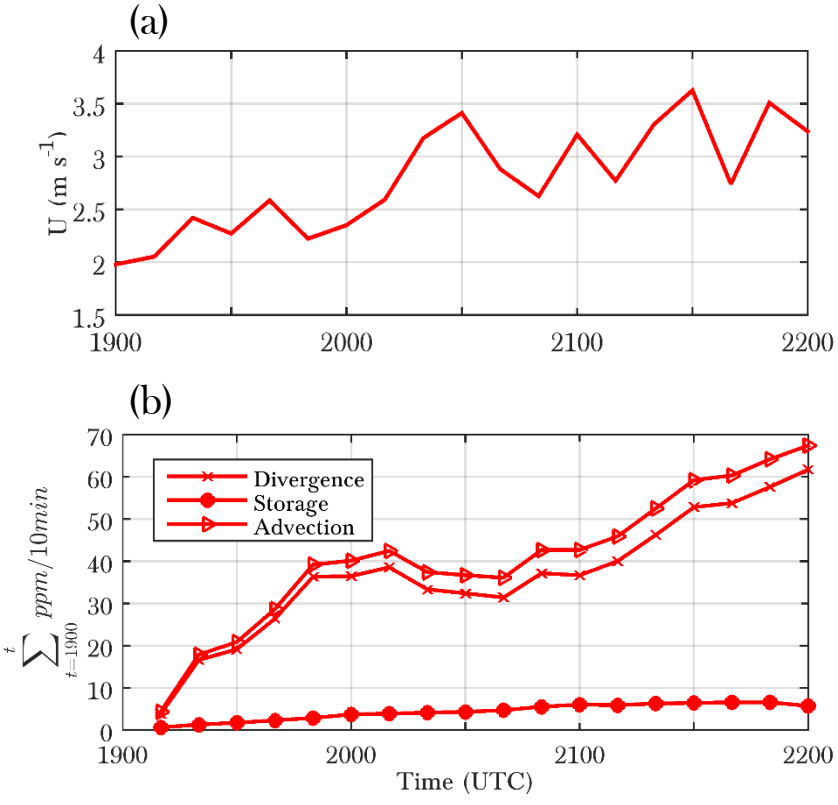

Figure 14. Time evolution between 1900 and 2200 UTC for the intense katabatic event, of (a) the wind speed (U) at 6 m, and (b) the different terms of the CO_2 budget from Eq. 6. Note that the cumulative sum from 1900 UTC is represented in (b), and that the advection term, which is negative, is shown in absolute values.